

Evaporation of a nonsingular Reissner-Nordström black hole and information loss problem

Kensuke Sueto¹ and Hirotaka Yoshino^{1,2}

¹*Department of Physics, Osaka Metropolitan University, Osaka 558-8585, Japan*

²*Nambu Yoichiro Institute of Theoretical and Experimental Physics (NITEP), Osaka Metropolitan University, Osaka 558-8585, Japan*

.....
One of the attractive solutions to the information loss problem is that the event horizon does not appear in the process of gravitational collapse and subsequent evaporation once the spacetime singularity is regularized by some mechanism, as pointed out by Hayward and Frolov. In this paper, we examine whether this Hayward-Frolov scenario holds for the evaporation of a charged black hole. The process of collapse and evaporation is modeled with the charged Vaidya spacetime and two kinds of regularization of the central singularity are considered. Analyzing the spacetime structure of the evaporating black hole, we find that the appropriately regularized evaporating Reissner-Nordström “black hole” has no event and Cauchy horizons, indicating the possibility that the Hayward-Frolov scenario may have sufficient generality as the solution to the information loss problem. In addition, the properties of the non-singular evaporating Reissner-Nordström black hole are examined in detail.
.....

Subject Index E31, E03, E05

1. Introduction

The theory of general relativity has broad applicability to gravitational phenomena such as cosmology, black holes and gravitational waves, but it is not expected to be a complete theory of gravity because the singularity theorems predict the formation of spacetime singularities in fairly generic situations such as inside of black holes. In a Schwarzschild spacetime, a spacelike singularity is located at $r = 0$, and the spacetime is not extendible beyond that singularity.

Another problem of general relativity arises if we consider the effects of quantum fields in a curved spacetime. Hawking has shown that the black hole emit quantum particles with a thermal spectrum, which is called the Hawking radiation [1, 2]. Due to this process, a black hole is expected to evaporate if the backreaction of the radiation is taken into account. This process appears to break the unitarity of quantum theories. Here, we briefly describe the reason following the argument of Ref. [3]. Figure 1 shows the typical Penrose diagram of the spacetime for the formation and the subsequent evaporation of a Schwarzschild black hole [2, 4, 5]. Let Σ , Σ_P , Σ' be spacelike hypersurfaces before the event horizon is formed, at the moment the black hole evaporates completely, and after the evaporation, respectively, as shown in the figure. Since there is no causal connection between the inside and the outside

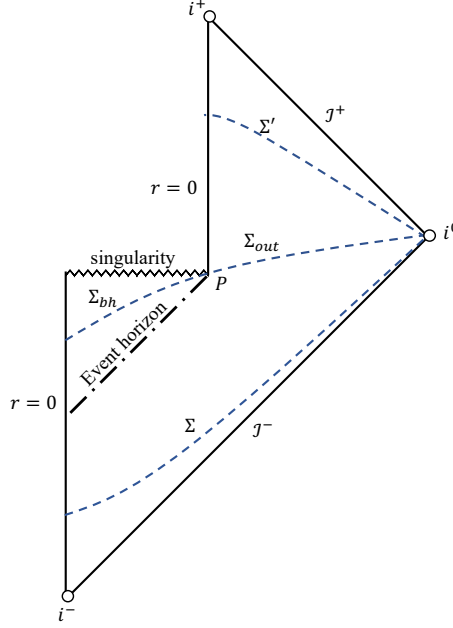


Fig. 1 Penrose diagram for the formation and the evaporation of a black hole.

of the event horizon, the hypersurface Σ_P can be divided as $\Sigma_P = \Sigma_{bh} + \Sigma_{out}$, where Σ_{bh} and Σ_{out} denote parts of the hypersurface in the inside and outside regions of the horizon, respectively. Since Σ_{bh} disappears as the black hole evaporates, the evolution from Σ to Σ' implies a transition from the pure state to the mixed state. This breaks the unitarity, which is the basic principle of quantum theories. This problem is called the black hole information loss problem pointed out by Hawking in 1976 [6], and since then, the information loss problem has been actively discussed.

Many solutions to the information loss problem have been proposed so far (see, e.g., [3, 7, 8] for reviews). In this paper, we would like to focus attention to the scenario proposed by Hayward [9]. The basic idea is as follows. In the example of the evaporation of a Schwarzschild black hole, the violation of unitarity is caused by the disappearance of the spacelike hypersurface inside of the event horizon due to the formation of a spacelike singularity. The singularity formation would occur because Einstein's equations, i.e. the equations of the classical theory of gravity, are applied to the regime where quantum gravity effects would become important. Many researchers would believe that the paradox should be resolved if a complete theory of quantum gravity appears. In such a complete theory, the spacetime singularity is expected to be resolved, and Hayward assumed that the spacetime structure is described with an effective metric without divergence of the curvature tensor. Hayward called such spacetime structure “the nonsingular black hole” and in this paper, we also call it “the regularized black hole”. Modeling the gravitational collapse and the subsequent evaporation of a black hole by combining Vaidya spacetimes with a naturally regularized metric at $r = 0$, the spacetime structure was shown to drastically change from that of Fig. 1. The resultant spacetime has no event horizon although an apparent horizon is present (see Fig. 5 of [9]). This model was independently reconstructed by Frolov (see arXiv 1st version of [10]), and hence, we call this scenario the *Hayward-Frolov scenario* in this paper. This scenario has an attractive feature

in that the information loss problem can be solved with a minimal change in the metric at the central singularity. See also Refs. [11–21] for models that share the similar features.¹

Here, we point out that whether this scenario holds for generic spacetimes must be questioned. For example, the Hayward-Frolov scenario has been studied just for spherically symmetric systems without electric charge. In realistic situations, a star under the gravitational collapse would be rotating, and hence, would have angular momentum, and the region outside of a collapsing star is expected to settle to a Kerr spacetime. The Kerr spacetime has two horizons at $r = r_{\pm} := M \pm \sqrt{M^2 - a^2}$, where M is the mass and Ma is the angular momentum. Here, $r = r_+$ is the event horizon, and $r = r_-$ corresponds to the Cauchy horizon. At the Cauchy horizon, the spacetime singularity is expected to develop if a perturbation is added due to the mass inflation [23–25], which corresponds to the fact that an observer crossing the Cauchy horizon would see phenomena of infinite duration of time in the outside region at an instant. Then, do we have to regularize the spacetime at a larger scale (i.e., near $r = r_-$) in the Hayward-Frolov scenario when the spacetime has the angular momentum? If so, does the resultant spacetime conserve information? Or, the resolution of the spacetime singularity at $r = 0$ is sufficient? Such a question is the basic motivation of this paper.

To study this problem, it is convenient to begin with a simpler model. The Reissner-Nordström spacetime with the mass M and the charge Q also possesses both the event horizon and the Cauchy horizon at $r = r_+$ and $r = r_-$, respectively, where $r_{\pm} = M \pm \sqrt{M^2 - Q^2}$. Since the Reissner-Nordström spacetime is spherically symmetric, it can be handled more easily compared to the Kerr spacetime, while it possesses the similar feature to the Kerr spacetime. For this reason, we consider the gravitational collapse and the subsequent evaporation of charged matter. The spacetime is modeled by combining charged Vaidya solutions with a regularized metric at the center.

Here, we have to comment on the existing works by Kaminaga [26] and Levin and Ori [27] which investigated the spacetime structure of a collapsing charged matter and its subsequent evaporation, without regularizing the metric (see also [28, 29]). They considered the cases where the spacetime has self-similarity. Kaminaga studied the simple case (called the model (A) in Ref. [27]) where the collapsing charged matter and the charged negative-energy Hawking particles continue to fall into the center, $r = 0$. Levin and Ori took account of the possibility that infalling charged matter and charged negative-energy Hawking particles might experience bounce towards the outward direction due to electromagnetic interactions that had been pointed out in Ref. [30] (see also Refs. [31–33]), and studied the Penrose diagram for such a case (called the model (B) in [27]). In both cases, a naked singularity appears in a spacetime.

Motivated by such existing studies and discussions, the purposes of this paper are the following three. First, we discuss the simplest regularization of the spacetime singularity at $r = 0$ of an ingoing charged Vaidya spacetime. Since the same discussion can be applied for the static spacetime, we first discuss the regularization of the Reissner-Nordström spacetime. We consider fairly general form of the metric functions, and derive the simplest one. The

¹ See also Ref. [22] for the discussion that pointed out the difficulty in realizing the Hayward-Frolov scenario within the framework of general relativity.

derived simplest metric turns out to correspond to the metric that is presented in Ref. [34] as an example of the regularized metric of the Reissner-Nordström spacetime.

Next, we study the spacetime structure for the collapse and the subsequent evaporation of a charged star with the regularized metric at the center. Due to a technical reason, we do not consider the bounce of the null charged matter, and hence, focus only on Kaminaga’s model, or the model (A). We consider two kinds of regularizations at the center. One is the regularization such that the self-similarity of Kaminaga’s model is maintained. In this case, the typical scale ℓ of the regularization is time dependent. It turns out that this method is not sufficient to resolve the information loss problem since the spacetime singularity still appears. The other is that the typical scale of the regularization ℓ is constant and does not depend on time. Since the constancy of ℓ violates the self-similarity of the spacetime, this case cannot be handled analytically and numerical calculations are required. In this case, the spacetime does not possess both the event horizon and the Cauchy horizon, and hence, has the ideal feature for resolving the information loss problem. Our result indicates that the Hayward-Frolov scenario would hold if an appropriate regularization is assumed.

Finally, we study the properties of evaporating non-singular Reissner-Nordström spacetime. Frolov pointed out interesting properties in an evaporating Hayward “black hole” spacetime without an event horizon, i.e. the existence of the repeller (or equivalently, the quasi-horizon) and the attractor of outgoing null geodesics [10]. Due to the existence of the attractor, extremely strong blueshift of outgoing photons occurs at the last stage of evaporation. We study how such properties depend on the charge in our system.

This paper is organized as follows. In the next section, we review the spacetime structures of the collapse of the charged matter and its evaporation studied by Kaminaga [26], since it is closely related to our study in this paper. In Sect. 3, we discuss how to regularize the metric of a Reissner-Nordström spacetime, and explain two methods of the regularization of charged Vaidya spacetimes that will be used in this paper. In Sect. 4, we study the self-similar model of the collapse and the evaporation of charged matter where the scale ℓ of the regularization of the central singularity is time dependent. In Sect. 5, the case where ℓ is time independent is analyzed. Section 6 is devoted to a summary and discussions. In Appendix A, the detailed calculation of the homothetic Killing vector field in the self-similar model is presented, and in Appendix B, how to solve for the location of the apparent horizons in Vaidya spacetimes is explained. We present the detailed calculations for the structures of the collapse domain in Appendix C. In Appendix D, calculations for the Riemann invariants of regularized charged Vaidya spacetimes are presented. Furthermore, we examine the properties of the Einstein tensor of regularized charged Vaidya spacetimes and in particular, discuss in which regions the null and dominant energy conditions are satisfied if these spacetimes are realized in the framework of general relativity. The characteristics of the apparent horizons in these spacetimes are also discussed. In Appendix E, we discuss how to connect the inner and outer domains, in which ingoing and outgoing Hawking fluxes are present, respectively, along the pair-creation surface. In Appendix F, we present the Penrose diagram that is drawn in a different method from that of the main text. Throughout the paper, we use the unit in which the speed of light and the gravitational constant are unity, $c = G = 1$.

2. Review of evaporation of a Reissner-Nordström black hole

A toy model for the collapse and evaporation of a charged star were presented by Kam-inaga [26] (see also Levin and Ori [27]) by cutting and gluing the ingoing and outgoing charged Vaidya spacetimes and the Reissner-Nordström spacetime. Here, we briefly review this model since it is closely related to our analysis in Sect. 4.

2.1. Charged Vaidya spacetimes

We begin with reviewing the charged Vaidya spacetimes [35]. The ingoing charged Vaidya spacetime is described by the metric

$$ds^2 = -F_-(v, r)dv^2 + 2drdv + r^2d\Omega^2 \quad (1)$$

with

$$F_-(v, r) = 1 - \frac{2M(v)}{r} + \frac{Q^2(v)}{r^2}, \quad (2)$$

where $d\Omega^2$ is the standard metric of a unit sphere, $d\Omega^2 = d\theta^2 + \sin^2\theta d\phi^2$, in the spherical-polar coordinates (θ, ϕ) . Here, the mass and charge functions, $M(v)$ and $Q(v)$, can be freely chosen. This metric describes the structure of a spherically symmetric spacetime with infalling charged null-matter fluid. The electromagnetic field is generated by the charged matter, and the only nonzero component of the electromagnetic field strength $\mathcal{F}_{\mu\nu}$ is

$$\mathcal{F}_{rv} = -\mathcal{F}_{vr} = \frac{Q(v)}{r^2}. \quad (3)$$

The energy-momentum tensor $T_{\mu\nu}$ is decomposed into two parts,

$$T_{\mu\nu} = T_{\mu\nu}^{(e)} + T_{\mu\nu}^{(m)}, \quad (4)$$

where $T_{\mu\nu}^{(e)}$ is the standard energy-momentum tensor for the electromagnetic field,

$$T_{\mu\nu}^{(e)} = \frac{1}{4\pi} \left(\mathcal{F}_{\mu\rho}\mathcal{F}_{\nu}{}^\rho - \frac{1}{4}g_{\mu\nu}\mathcal{F}_{\rho\sigma}\mathcal{F}^{\rho\sigma} \right), \quad (5)$$

and $T_{\mu\nu}^{(m)}$ is the matter part. For the field strength given by Eq. (3), $T_{\mu\nu}^{(e)}$ takes the form

$$T^{(e)\mu}{}_{\nu} = \text{diag}(-\tilde{\rho}, \tilde{p}_r, \tilde{p}_\theta, \tilde{p}_\phi) \quad (6)$$

with

$$\tilde{\rho} = -\tilde{p}_r = \tilde{p}_\theta = \tilde{p}_\phi = \frac{Q^2}{8\pi r^4}, \quad (7)$$

where $\tilde{\rho}$, \tilde{p}_r , \tilde{p}_θ , and \tilde{p}_ϕ denote the energy density and the pressures in the r , θ , and ϕ directions due to the electromagnetic field, respectively. In order to express the matter part, it is convenient to introduce the ingoing radial null vector

$$k^\mu = -(\partial_r)^\mu, \quad (8)$$

and its dual vector $k_\mu = -(dv)_\mu$. In terms of k^μ , $T_{\mu\nu}^{(m)}$ is expressed as

$$T_{\mu\nu}^{(m)} = \tilde{\nu} k_\mu k_\nu, \quad (9)$$

with

$$\tilde{\nu} = \frac{1}{4\pi r^2} \left(M' - \frac{QQ'}{r} \right). \quad (10)$$

Here, the prime (\prime) denotes the ordinary derivative, i.e. $M' = dM/dv$ in this case. This matter is the charged null fluid having the energy density $\tilde{\nu}$ (for the observer whose four-velocity

v^μ satisfies $k^\mu v_\mu = -1$) which propagates from $r = \infty$ to $r = 0$ along $v = \text{constant}$ surfaces. From the Maxwell equation, the four-electric current is given as

$$j^\mu = -\frac{1}{4\pi} \nabla_\nu \mathcal{F}^{\nu\mu} = \frac{Q'}{4\pi r^2} k^\mu, \quad (11)$$

which is a null vector. This reflects the fact that the charged null matter carries the electric charge at the speed of light.

Similarly, the metric of the outgoing Vaidya spacetime is given by

$$ds^2 = -F_+(u, r) du^2 - 2drdu + r^2 d\Omega^2, \quad (12)$$

where

$$F_+(u, r) = 1 - \frac{2M(u)}{r} + \frac{Q^2(u)}{r^2}. \quad (13)$$

This metric describes the structure of a spacetime with outgoing charged null-matter fluid.

2.2. Kaminaga's self-similar model

A model of an evaporating charged black hole due to Hawking radiation was proposed by Kaminaga [26]. This model was called the model (A) by Levin and Ori [27], and here, we give a detailed review on this model because the extension of this model will be discussed in Sect. 4. The setup of the system in this paper is slightly different from those of Refs. [26] and [27].

2.2.1. Setup. In this model, a charged black hole is formed by the gravitational collapse of charged null-matter fluid that is described by the charged Vaidya solution. After the collapse, Hawking particles are assumed to be created at a timelike hypersurface that is slightly outside of the apparent horizon. Outside of that timelike hypersurface, the Hawking particles constitute an outgoing null matter fluid with positive outgoing energy flux, while inside of that timelike hypersurface, they constitute ingoing null-matter fluid with (initially) ingoing negative energy flux.² The outside and inside regions are modeled by the outgoing and ingoing charged Vaidya spacetimes, respectively.

It is convenient to study the ingoing charged Vaidya spacetime with the mass function³

$$M(v) = \begin{cases} 0 & (v \leq -v_i), \\ M_0(1 + v/v_i) & (-v_i \leq v \leq 0), \\ M_0(1 - v/v_f) & (0 \leq v \leq v_f), \\ 0 & (v \geq v_f), \end{cases} \quad (14)$$

and the charge function,

$$Q(v) = qM(v). \quad (15)$$

² We commented “initially” because due to the matter part of the energy-momentum tensor of Eq. (9), the energy density changes its sign at some certain radius. This property plays an important role in the discussion of Levin and Ori [27].

³ Precisely speaking, Kaminaga adopted the case of $v_i = 0$ (i.e., instantaneous collapse) in Ref. [26]. Also, the period where the mass function linearly decreases is assumed to end before $v = v_f$, and $M(v)$ suddenly jumps from a positive value to zero. For this reason, the presented Penrose diagram is different from Fig. 5 of this paper. The mass function of Levin and Ori of Ref. [27] is the same as Eq. (14) for $v > 0$, but they assumed the spacetime to be initially the Reissner-Nordström spacetime (without the gravitational collapse).

Since we consider the formation of a sub-extremal black hole, $|q| < 1$ is assumed. Once the structure of this ingoing charged Vaidya spacetime is clarified, the spacetime of an evaporating charged black hole can be easily constructed with a minor modification by cutting and gluing this spacetime, the outgoing charged Vaidya spacetime, and the Reissner-Nordström spacetime (interested readers are referred to Fig. 4 in advance). Note that the linear dependence of $M(v)$ and $Q(v)$ on the advanced time v is assumed by a technical reason. With this choice of functions, the spacetime becomes self-similar and the analysis becomes easy (see below). In the mass function of Eq. (14), on the one hand, the gravitational collapse occurs in the domain $-v_i \leq v \leq 0$, and we call this domain the collapsing phase. On the other hand, the negative energy flux of the ingoing Hawking particles is present in the domain $0 \leq v \leq v_f$, and we call this domain the evaporating phase. The other domains are the Minkowski spacetimes. We focus our attention particularly to the domain $0 \leq v \leq v_f$ where the ingoing energy flux is negative, because that domain is expected to describe the spacetime structure of the evaporating black hole with backreaction.

2.2.2. Double null coordinates. In the domain $0 \leq v \leq v_f$, we introduce two new coordinates \tilde{v} and R by

$$\tilde{v} = \frac{M(v)}{M_0}, \quad R = \frac{r}{M(v)}. \quad (16)$$

Note that $0 \leq v \leq v_f$ corresponds to $1 \geq \tilde{v} \geq 0$. Then, the function $F_-(v, r)$ in the metric of Eq. (1) is rewritten as

$$F_-(v, r) = 1 - \frac{2}{R} + \frac{q^2}{R^2} =: f(R). \quad (17)$$

In these coordinates, the metric becomes

$$ds^2 = -M_0^2 \alpha \tilde{v} (f\alpha + 2R) d\tilde{v} \left(\frac{d\tilde{v}}{\tilde{v}} + \frac{2dR}{f\alpha + 2R} \right) + r^2 d\Omega^2, \quad (18)$$

where α denotes the duration of evaporation normalized by the initial mass,

$$\alpha = v_f/M_0. \quad (19)$$

From this formula, the retarded time u can be introduced by

$$u = \ln \tilde{v} + \int \frac{2dR}{f\alpha + 2R}. \quad (20)$$

Then, in the double null coordinates (u, \tilde{v}) , the metric is expressed as

$$ds^2 = -M_0^2 \alpha \tilde{v} (f\alpha + 2R) du d\tilde{v} + r^2 d\Omega^2. \quad (21)$$

The spacetime structure changes drastically depending on the number of zeros of the function $f\alpha + 2R$. The equation $f\alpha + 2R = 0$ is rewritten as

$$-\frac{1}{\alpha} = \frac{R^2 - 2R + q^2}{2R^3} =: y(R). \quad (22)$$

The graph of the function $y(R)$ is shown in Fig. 2 for the case $q = 0.6$. $y(R)$ takes extremal values at $R = R_{\pm} := 2 \pm \sqrt{4 - 3q^2}$, and $y(R_-) < 0$ and $y(R_+) > 0$ are satisfied. Since α is a positive constant, the left-hand side of Eq. (22) is negative, and Eq. (22) has one, two,

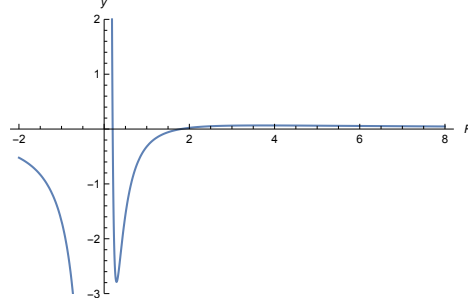


Fig. 2 The graph of $y(R)$ for the case $q = 0.6$.

and three solutions in the cases that $1/\alpha > |y(R_-)|$, $1/\alpha = |y(R_-)|$, and $1/\alpha < |y(R_-)|$, respectively, where

$$|y(R_-)| = -\frac{2 - q^2 - \sqrt{4 - 3q^2}}{(2 - \sqrt{4 - 3q^2})^3}. \quad (23)$$

When $f\alpha + 2R = 0$ has one root, on the one hand, the root R_0 is negative, $R_0 < 0$, and the function $f\alpha + 2R$ is always positive in the range $0 < R < \infty$. In this case, the null coordinate u spans the whole domain of $1 \geq \tilde{v} \geq 0$. On the other hand, if $f\alpha + 2R = 0$ has three roots, which are denoted by R_0 , R_C^- and R_C^+ with $R_0 < 0 < R_C^- < R_C^+$, the coordinate u diverges to $\mp\infty$ in the limit $R \rightarrow R_C^\pm$ with a fixed \tilde{v} . Explicitly, the relation between u , \tilde{v} , and R is written as

$$u = \ln \tilde{v} + \frac{1}{\kappa_0} \ln |R - R_0| - \frac{1}{\kappa_-} \ln |R - R_C^-| + \frac{1}{\kappa_+} \ln |R - R_C^+|, \quad (24)$$

where

$$\kappa_0 = \frac{(R_C^+ - R_0)(R_C^- - R_0)}{R_0^2}, \quad (25a)$$

$$\kappa_\pm = \frac{(R_C^+ - R_C^-)(R_C^\pm - R_0)}{(R_C^\pm)^2}. \quad (25b)$$

The divergence of u in the limit $R \rightarrow R_C^\pm$ is just the coordinate effect. In fact, the continuous null coordinates U_+ and U_- across $R = R_C^+$ and $R = R_C^-$, respectively, can be locally introduced by

$$U_\pm = \begin{cases} \exp(\pm \kappa_\pm u) & (R > R_C^\pm), \\ -\exp(\pm \kappa_\pm u) & (R < R_C^\pm), \end{cases} \quad (26)$$

in which the metric takes the regular form

$$ds^2 = -\frac{2M_0^2 \alpha \tilde{v}^{1 \mp \kappa_\pm} (R - R_0)^{1 \mp \kappa_\pm / \kappa_0} |R - R_C^\mp|^{1 + \kappa_\pm / \kappa_\mp}}{\kappa_\pm R^2} dU_\pm d\tilde{v}. \quad (27)$$

The important feature is that if we decrease \tilde{v} to zero for a fixed u in the domain $0 < R < R_C^+$, the value of R approaches R_C^- because κ_0 , κ_+ and κ_- are all positive in Eq. (24). Since this limit corresponds to $r = 0$ because of the definition of R of Eq. (16), there is a null singularity. This feature is used in drawing the Penrose diagram later. In Section 5.1, we present the behavior of outgoing null geodesics, each of which gives a u -constant surface, in the (v, r) -plane for the cases that the homothetic Killing horizons are present and absent. This would help us to understand the properties of this spacetime.

2.2.3. Homothetic Killing vector field. In the domain where $M(v)$ changes linearly, a homothetic Killing vector field ξ^μ is present. The homothetic Killing vector field is the vector field that satisfies the equation

$$\nabla_\mu \xi_\nu + \nabla_\nu \xi_\mu = K g_{\mu\nu} \quad (28)$$

for some constant K (if K is not a constant, ξ^μ is called the conformal Killing vector field). The presence of the homothetic Killing field is proven in Appendix A. The contravariant components of the homothetic Killing vector is given by

$$\xi^\mu = -(1, \tilde{v}, 0, 0), \quad (29)$$

in the $(u, \tilde{v}, \theta, \phi)$ coordinates and satisfies Eq. (28) with $K = -2$. The norm of this vector is

$$g_{\mu\nu} \xi^\mu \xi^\nu = -M_0^2 \alpha \tilde{v}^2 (f\alpha + 2R). \quad (30)$$

A homothetic Killing horizon is defined as a surface on which ξ^μ becomes null, and its location satisfies $f\alpha + 2R = 0$ or $\tilde{v} = 0$ in the present system. Whether there exist homothetic Killing horizons except for $\tilde{v} = 0$ depends on the parameter α and q . If α is sufficiently large and q^2 is sufficiently small, there exist two solutions for $f\alpha + 2R = 0$ in the domain $R > 0$ which are R_C^\pm introduced above.

Here, we point out that the vector field ξ^μ is tangent to the R -constant hypersurfaces as can be checked from Eq. (29) and the definition of u of Eq. (20). Due to the spherical symmetry, the characteristic of ξ^μ (i.e., timelike, null, or spacelike) and that of an R -constant hypersurface are identical to each other. Therefore, we find that ξ^μ and R -constant hypersurfaces are (i) timelike if $f\alpha + 2R > 0$; (ii) null if $f\alpha + 2R = 0$; and (iii) spacelike if $f\alpha + 2R < 0$. In the case that a homothetic Killing horizon does not exist except for $\tilde{v} = 0$, all R -constant hypersurfaces are timelike. In the case that the two homothetic Killing horizons are present except for $\tilde{v} = 0$, R -constant hypersurfaces are timelike for $0 < R \leq R_C^-$ and $R_C^+ < R$, null for $R = R_C^\pm$, and spacelike for $R_C^- < R < R_C^+$.

2.2.4. Trapped region. Suppose photons are emitted from r -constant surface at some moment in both inward and outward radial directions. The region where both ingoing and outgoing null geodesic congruences have negative expansion is called the trapped region, and the outermost boundary of that region is called the apparent horizon. In the present spacetime, the expansion of ingoing null geodesic congruence is always negative. As shown in Appendix B, the expansion of outgoing null geodesic congruence is proportional to $f(R)$, which is defined in Eq. (17). The boundaries of the trapped region are obtained by solving the equation $f(R) = 0$. If $q^2 < 1$, there are two solutions for this equation, which are

$$R_A^\pm = 1 \pm \sqrt{1 - q^2}. \quad (31)$$

The surfaces $R = R_A^-$ and $R = R_A^+$ correspond to the inner boundary of the trapped region and the apparent horizon, respectively. Following Ref. [10], we call them the inner and outer apparent horizons in this paper.

2.2.5. (v, r) -diagram. In order to understand the spacetime structure, it is very helpful to present the outgoing null geodesics, homothetic Killing horizons, and the apparent horizons in the (v, r) -plane. We call such a diagram the “ (v, r) -diagram”. Although the outgoing null

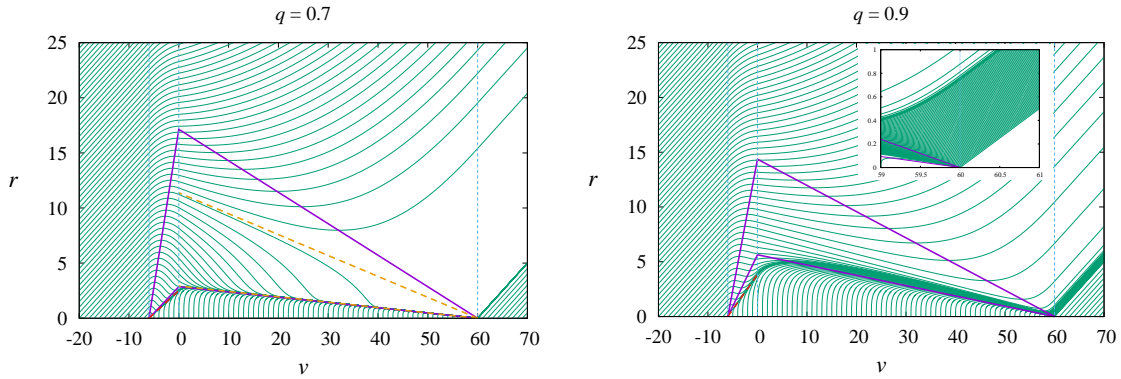


Fig. 3 Outgoing null geodesics (thin green curves) and the boundary of the trapped region (closed purple lines) for the ingoing charged Vaidya spacetime (Kaminaga’s model) in the cases $q = 0.7$ (left panel) and $q = 0.9$ (right panel). The parameters $M_0 = 10$, $v_i = 6$, and $v_f = 60$ are adopted. The red dashed line in each panel indicate the homothetic Killing horizon in the collapsing phase. The orange dashed lines in the left panel shows the homothetic Killing horizons in the evaporating phase (no homothetic Killing horizon exists in the evaporating phase in the right panel). The vertical dotted lines in each panel indicate $v = -v_i$, 0 , and v_f from left to right.

geodesics are given by u -constant surfaces determined by Eq. (20), it is useful to develop a code to generate outgoing null geodesics numerically, since non-self-similar spacetimes, for which no analytic solution to the geodesic equation is present, will be studied later. From the null condition, radial outgoing null geodesics satisfy

$$\frac{dr}{dv} = \frac{F_-(v, r)}{2}. \quad (32)$$

This differential equation can be solved numerically in the domain $r \geq 0$ using the Runge-Kutta method. Note that there is a difficulty in solving for the outgoing null geodesics that is emitted from the curvature singularity at $r = 0$. In fact, the equation is singular at the center $r = 0$ as

$$\frac{dr}{dv} = \frac{1}{2} \left(1 - \frac{2M(v)}{r} + \frac{q^2 M(v)^2}{r^2} \right), \quad (33)$$

in the range $-v_i < v < v_f$. We avoid this singularity by adopting $x = r^3$. The equation for x is

$$\frac{dx}{dv} = \frac{3}{2} \left[x^{2/3} - 2M(v)x^{1/3} + q^2 M(v)^2 \right], \quad (34)$$

and after solving this equation, we obtain $r(v) = x(v)^{1/3}$.

Figure 3 shows the (v, r) -diagrams for $q = 0.7$ (left panel) and 0.9 (right panel). In the diagrams, behavior of outgoing null geodesics (thin green curves) and the boundary of the trapped region (thick purple lines or curve) are shown. In both panels, the parameters $M_0 = 10$, $v_i = 6$, and $v_f = 60$ are adopted. In the left panel for $q = 0.7$, there are two homothetic Killing horizons in the evaporating phase, and they are indicated by orange dashed lines. These two homothetic Killing horizons coincide with two of the outgoing null geodesics. The outer homothetic Killing horizon clearly separates the outgoing null geodesics that escape

to infinity and those trapped inside of it, and hence, it is the event horizon as well. Since the null geodesics recede from the outer homothetic Killing horizon, it plays a role of the repeller of outgoing null geodesics. Frolov called such a repeller “quasi-horizon” (see Fig. 2 of [10]) and showed that it is well approximated by the positions where d^2r/dv^2 becomes zero in general ingoing Vaidya spacetimes, where the outgoing null geodesics are given by $r = r(v)$ (see also Ref. [19] for more detailed discussions on such a separatrix). The trapped outgoing null geodesics are strongly attracted by the inner homothetic Killing horizon, and therefore, the inner homothetic Killing horizon plays a role of the attractor. All outgoing null geodesics within the outer homothetic Killing horizon plunge into the singularity at $(v, r) = (v_f, 0)$. This means that the singularity at $(v, r) = (v_f, 0)$ has an extended structure in the u direction, and thus, that singularity is a null singularity.

In the right panel for the case of $q = 0.9$, the homothetic Killing horizons do not exist. As a result, there is no event horizon in this spacetime, and all outgoing null geodesics escape to infinity. The absence of the inner homothetic Killing horizon implies the non-existence of the attractor. Although outgoing null geodesics tend to gather around the inner boundary of the trapped region, the gathering is not sufficiently strong to form an attractor. Since no outgoing geodesic plunges into the singularity at $(v, r) = (v_f, 0)$ from $v < v_f$, it does not have an extended structure in the u direction.

In each of the left and right panels, the red dashed line represents the homothetic Killing horizon in the collapsing phase (see Appendix C for an analytic study for the spacetime structure of the collapsing phase). This homothetic Killing horizon is an attractor of outgoing null geodesics in the future direction. As a result, only one outgoing null geodesic is emitted from the point $(v, r) = (-v_i, 0)$. This means that the singularity at this point does not have an extended structure in the u -direction in both cases of $q = 0.7$ and 0.9 .

2.2.6. Penrose diagram. Summarizing the above informations, we can now draw the Penrose diagram. We suppose that q^2 is smaller than one, and hence, the apparent horizon forms. The existence of the homothetic Killing horizon depends on the value of α . Below, we first show the Penrose diagram given by the ingoing charged Vaidya spacetime with the mass function of Eq. (14), and then, discuss how to modify that diagram in order to obtain the diagram for an evaporating charged black hole.

The left panel of Fig. 4 shows the Penrose diagram for the ingoing charged Vaidya spacetime in the case that the homothetic Killing horizon does not exist except for $\tilde{v} = 0$, which corresponds to the right panel of Fig. 3. The R -constant surfaces are shown by dotted curves, and they are all timelike in the evaporating phase. All of the R -constant surfaces shrink to one point, $r = \tilde{v} = 0$. The boundaries of the trapped region, $R = R_A^\pm$, are shown by solid curves.⁴ The trapped region shrinks as \tilde{v} is decreased and becomes pointlike at $\tilde{v} = r = 0$. There appears a timelike singularity at the center, $r = 0$. The event horizon is absent, and the spacetime possesses the naked singularity that is visible to distant observers.

⁴ In the collapsing phase, the both inner and outer boundaries of the trapped region are spacelike, and in the evaporating phase they are both timelike. One might wonder whether this result is consistent with Hayward’s theorem [36] which states that if the null energy condition holds in general relativity, an outer trapping horizon is spacelike and an inner trapping horizon is timelike. Our result is consistent with Hayward’s result, as presented in Appendix D.

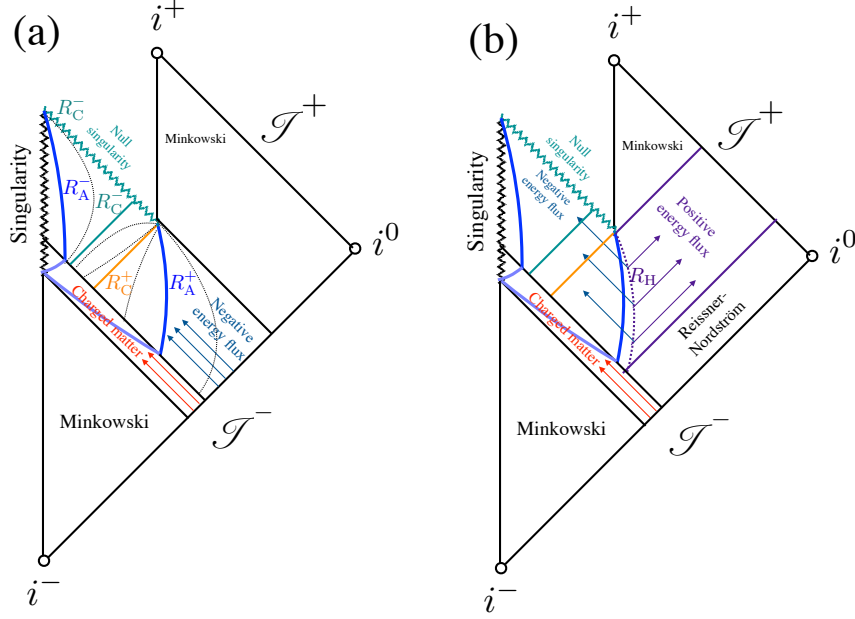


Fig. 5 Penrose diagrams for the charged Vaidya spacetime (left panel) and the model of the Hawking radiation (right panel) in the case that homothetic Killing horizons form.

In Sects. 4 and 5, we consider how these diagrams are changed if we regularize the singularity at the center keeping and breaking the self-similar property of the spacetime, respectively.

3. Regularization of Reissner-Nordström metric

In this section, we discuss how to regularize the singularity at the center of electrically charged spacetimes. First we study the regularization of a static Reissner-Nordström spacetime, since the same regularization method can be applied to the ingoing charged Vaidya spacetime as well. Then, we present the regularization of the ingoing charged Vaidya spacetime that will be used in subsequent sections.

3.1. A method of constructing nonsingular static Reissner-Nordström spacetime

Let us consider the metric of a static spacetime in the ingoing Eddington-Finkelstein coordinates,

$$ds^2 = -F(r)dv^2 + 2dvdr + r^2d\Omega^2. \quad (35)$$

For a Schwarzschild spacetime, the function $F(r)$ takes the well-known form, $F(r) = 1 - 2M/r$. This function diverges at $r = 0$, and it is the origin of the curvature singularity at $r = 0$. Hayward [9] considered the regularized form as

$$F(r) = 1 - \frac{2Mr^2}{r^3 + 2M\ell^2}. \quad (36)$$

Then, the central singularity disappears, and there is a regular center at $r = 0$. Let us consider the charged version of the regularized function of $F(r)$.

In Ref. [34], Frolov presented an example of a nonsingular Reissner-Nordström metric. Here, considering a rather general form of the metric function, we shall show that Frolov's

metric is the simplest one (see Ref. [19] for a similar discussion in the uncharged case). The Reissner-Nordström metric is given by Eq. (35) with

$$F(r) = 1 - \frac{2M}{r} + \frac{Q^2}{r^2}, \quad (37)$$

where M is the Arnowitt-Deser-Misner mass and Q is the total charge. Here, we would like to modify the function $F(r)$ in order to make the spacetime nonsingular at $r = 0$. Following Ref. [34], the function $F(r)$ is assumed to behave near $r \sim 0$ as

$$F(r) \sim 1 + \varepsilon \frac{r^2}{\ell^2}, \quad (38)$$

where ε is $+1$ or -1 and ℓ is the cut-off parameter that gives the typical scale of regularization. We assume $F(r)$ to be a ratio of polynomials with respect to r of the order n .

$$F(r) = 1 - \frac{\sum_{k=0}^{n-1} b_k r^k}{\sum_{j=0}^n a_j r^j}. \quad (39)$$

From the condition of Eq. (38), we have $F(0) = 1$, $F'(0) = 0$, $F''(0) = 2\varepsilon/\ell^2$, and this implies $b_0 = 0, b_1 = 0, a_0 = -\varepsilon b_2 \ell^2$. For large r , $F(r)$ can be expanded as

$$F(r) \approx 1 - \frac{b_{n-1}}{r} + \frac{a_{n-1}b_{n-1} - b_{n-2}}{r^2} - \frac{b_{n-3} - a_{n-1}b_{n-2} - b_{n-1}(a_{n-2} - a_{n-1}^2)}{r^3} + O\left(\frac{1}{r^4}\right). \quad (40)$$

Requiring this formula to coincide with the Reissner-Nordström metric up to the order of $1/r^3$ for large r , we obtain

$$b_{n-1} = 2M, \quad (41a)$$

$$a_{n-1}b_{n-1} - b_{n-2} = Q^2, \quad (41b)$$

$$b_{n-3} - a_{n-1}b_{n-2} - b_{n-1}(a_{n-2} - a_{n-1}^2) = 0. \quad (41c)$$

These conditions constitute a nonsingular Reissner-Nordström metric.

First, we consider the case of $n = 3$. Since $b_1 = b_0 = 0$ holds in general, Eqs. (41a)–(41c) fixes the coefficients as

$$a_1 = \left(\frac{Q^2}{2M}\right)^2, \quad a_2 = \frac{Q^2}{2M}, \quad b_2 = 2M, \quad (42)$$

and thus, the function $F(r)$ is determined as

$$F(r) = 1 - \frac{2Mr^2}{r^3 + \frac{Q^2}{2M}r^2 + \left(\frac{Q^2}{2M}\right)^2 r - 2\varepsilon M \ell^2}. \quad (43)$$

However, this function is not reduced to the Reissner-Nordström metric in the limit of $\ell \rightarrow 0$. Therefore, we cannot construct an appropriate nonsingular Reissner-Nordström metric in the case of $n = 3$.

Next, we consider the case of $n = 4$. The conditions of Eqs. (41a)–(41c) are written as

$$a_2 = \frac{Q^2}{2M}a_3, \quad b_2 = 2Ma_3 - Q^2, \quad b_3 = 2M, \quad (44)$$

and this leads to

$$F(r) = 1 - \frac{2Mr^3 - (Q^2 - 2Ma_3)r^2}{r^4 + a_3r^3 + \frac{Q^2}{2M}a_3r^2 + a_1r + \varepsilon(Q^2 - 2Ma_3)\ell^2}. \quad (45)$$

There are two unfixed parameters a_1 and a_3 , and we require that $F(r)$ coincide with Eq. (36) of the Hayward model in the uncharged case. Since $F(r)$ is

$$F(r) = 1 - \frac{2Mr^3 + 2Ma_3r^2}{r^4 + a_3r^3 + a_1r - 2\varepsilon Ma_3\ell^2}, \quad (46)$$

for $Q = 0$, we have $a_3 = 0$, and thus

$$F(r) = 1 - \frac{2Mr^2}{r^3 + a_1}. \quad (47)$$

Comparing this equation with the Hayward model, the value of a_1 is determined as $a_1 = 2M\ell^2$. As a result, we have to choose $\varepsilon = +1$ in Eq. (45) to avoid divergence of $F(r)$, and

$$F(r) = 1 - \frac{(2Mr - Q^2)r^2}{r^4 + (2Mr + Q^2)\ell^2} \quad (48)$$

is the simplest model of the nonsingular Reissner-Nordström spacetime. The function $F(r)$ behaves as

$$F(r) \approx \begin{cases} 1 - \frac{r^2}{\ell^2} + \frac{r^5}{2\ell^4 M} + O(r^8) & (Q = 0); \\ 1 + \frac{r^2}{\ell^2} - \frac{4Mr^3}{\ell^2 Q^2} + O(r^4) & (Q \neq 0), \end{cases} \quad (49)$$

in the neighborhood of $r = 0$. In Hayward's spacetime with $Q = 0$, the difference of the metric from the exact dS metric is $O(r^5)$, and hence, the geometry is well approximated by the dS spacetime. In the case of $Q \neq 0$, although the metric around $r = 0$ resembles that of the anti-de Sitter (AdS) spacetime, its difference from the exact AdS metric is $O(r^3)$, and hence, the approximation is not as good as the Hayward case. We will come back to this point later.

3.2. Global structure of nonsingular static Reissner-Nordström spacetime

Here we analyze the locations of the horizons of the nonsingular Reissner-Nordström spacetime. The event and Cauchy horizons exist at positions satisfying $F(r) = 0$, and this equation is expressed as

$$r^4 - 2Mr^3 + Q^2r^2 + 2M\ell^2r + Q^2\ell^2 = 0. \quad (50)$$

Introducing the normalized variables $\tilde{r} = r/M$, $\tilde{\ell} = \ell/M$, $q = Q/M$, we can easily rewrite Eq. (50) as

$$\tilde{\ell}^2 = -\frac{\tilde{r}^2(\tilde{r} - \tilde{r}_0^+)(\tilde{r} - \tilde{r}_0^-)}{q^2 + 2\tilde{r}}, \quad (51)$$

where $\tilde{r}_0^\pm = 1 \pm \sqrt{1 - q^2}$. It can be seen that \tilde{r}_0^\pm are the event and Cauchy horizons of the original Reissner-Nordström spacetime (in the case of $\tilde{\ell} = 0$). Denoting the right-hand side

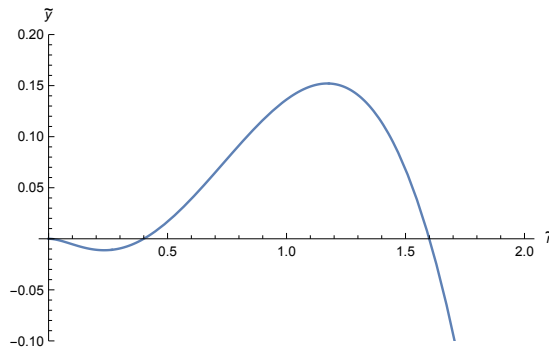


Fig. 6 The behavior of the function $\tilde{y}(\tilde{r})$ for $q = 0.8$.

of Eq. (51) as $\tilde{y}(\tilde{r})$, the graph of $\tilde{y}(\tilde{r})$ can be drawn as shown in Fig. 6 for the case of $q < 1$. With this figure, the radial positions of the event and Cauchy horizons, \tilde{r}_H^+ and \tilde{r}_H^- , can be obtained as the values of \tilde{r} of the intersection points of the curve $\tilde{y} = \tilde{y}(\tilde{r})$ and the line $\tilde{y} = \tilde{\ell}^2$. As a result, we have the relation $\tilde{r}_0^- < \tilde{r}_H^- < \tilde{r}_H^+ < \tilde{r}_0^+$.

Here we compare the Hayward model and the nonsingular Reissner-Nordström spacetime obtained here. The Hayward spacetime possesses two horizons, and the inner horizon is formed around $r = \ell$ due to the fact that the central region behaves like the de Sitter (dS) spacetime. By contrast, in the nonsingular Reissner-Nordström spacetime, the central region behaves like an AdS spacetime because $F(0) \rightarrow +\infty$ in the limit $r \rightarrow 0$ in the original Reissner-Nordström spacetime, and $F(0) = 1$ is required for nonsingular black holes. As a result, $F(r) = 0$ has two solutions, $r = \tilde{r}_H^+ M$ and $\tilde{r}_H^- M$, in the vicinity of the two horizons of the original Reissner-Nordström spacetime. Therefore, the global structure of a nonsingular Reissner-Nordström spacetime is similar to that of the original Reissner-Nordström spacetime except that the point $r = 0$ is no longer a curvature singularity.

If we choose a fine-tuned value of q , we can also consider a situation with only one degenerate horizon, but we will not consider such a situation in this paper.

3.3. Geometrical properties of the regularized spacetime

In order to realize the regularized spacetimes, there are two possibilities. One is that the theory of gravity is modified from the theory of general relativity. The other is that the theory of gravity is given by general relativity and the properties of matter (and therefore, the energy-momentum tensor) are changed. In this paper, we adopt the former possibility and do not care about whether such a spacetime is realized within the framework of general relativity. Nevertheless, it would be interesting to examine the properties of the energy-momentum tensor of this spacetime in the case that this spacetime is realized in general relativity, because such an analysis would deepen our understanding on the geometrical properties of this spacetime. For this reason, we examine the properties of the Einstein tensor here.

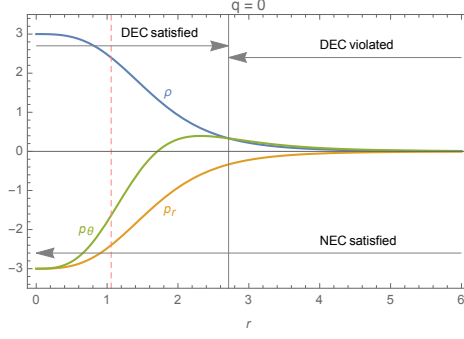


Fig. 7 Behavior of ρ , p_r , and p_θ for the Hayward spacetime with $M = 5$ and $\ell = 1$ as functions of r . The regions where the NEC and DEC are satisfied/violated are also shown. The red vertical dashed line shows the location of the inner horizon, while the outer horizon is outside of this figure.

We adopt the tetrad basis $(e^a)_\mu$ ($a = 0, 1, 2, 3$) as

$$(e^0)_\mu = \left(-\frac{1+F}{2}, 1, 0, 0 \right), \quad (52a)$$

$$(e^1)_\mu = \left(\frac{1-F}{2}, 1, 0, 0 \right), \quad (52b)$$

$$(e^2)_\mu = (0, 0, r, 0), \quad (52c)$$

$$(e^3)_\mu = (0, 0, 0, r \sin \theta), \quad (52d)$$

in the (v, r, θ, ϕ) coordinates, and consider the tetrad components of the Einstein tensor $G^{ab} = G^{\mu\nu}(e^a)_\mu(e^b)_\nu$. It is written in the form

$$G^{ab} = \text{diag}(\rho, p_r, p_\theta, p_\phi), \quad (53)$$

(which is called the canonical form of type I [37], see also [38]) where

$$\rho = -p_r = \frac{1 - F - rF_{,r}}{r^2}, \quad (54a)$$

$$p_\theta = p_\phi = \frac{F_{,r}}{r} + \frac{F_{,rr}}{2}. \quad (54b)$$

With this quantity, we can examine the property of the energy-momentum tensor in the case that the regularized spacetime is realized in the framework of general relativity with unordinary matter. In particular, we focus on the null energy condition (NEC) and the dominant energy condition (DEC). Assuming the Einstein equation, the NEC is $G_{\mu\nu}k^\mu k^\nu \geq 0$ for an arbitrary null vector k^μ , and the DEC is that $-G^\mu{}_\nu v^\mu$ is a future-directed timelike or null vector for an arbitrary future-directed timelike vector v^μ (e.g., [37]). The NEC is equivalent to

$$\rho + p_i \geq 0 \quad (55)$$

for $i = r, \theta, \phi$, and the DEC is equivalent to

$$\rho \geq |p_i|. \quad (56)$$

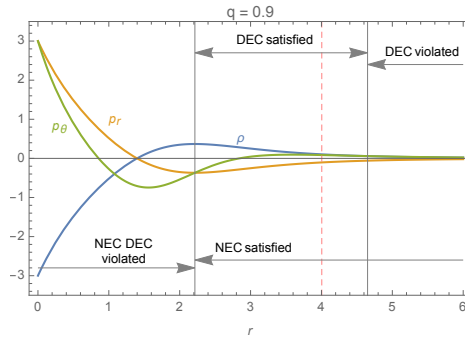


Fig. 8 The same as Fig. 7 but for charged regularized spacetime with $q = 0.90$.

Figure 7 shows the behavior of ρ , p_r , and p_θ for the Hayward spacetime with $M = 5$ and $\ell = 1$ as functions of r . These quantities decay as r is increased. ρ approaches $3/\ell^2$ and p_θ and p_r approach $-3/\ell^2$ in the limit $r \rightarrow 0$, and they are approximately constant in the neighborhood of $r = 0$. This is because the difference of Hayward's metric from the dS metric is $O(r^5)$ from Eq. (49), and hence, the deviation of the Einstein tensor from the cosmological term is $O(r^3)$. This confirms the fact that the Hayward spacetime is well approximated by a dS spacetime around the center. Although the NEC is satisfied in all regions, the DEC is violated at distant region because the value of p_θ exceeds that of ρ there. See also Ref. [39] for more study on the energy conditions of the Hayward spacetime and other regular black hole spacetimes.

Figure 8 shows the case of $q = 0.9$ for the case $M = 5$ and $\ell = 1$. In contrast to the case $q = 0.0$, ρ approaches $-3/\ell^2$, and p_θ and p_r approach $3/\ell^2$ at $r \rightarrow 0$. In this sense, the central point satisfies the Einstein equation with a negative cosmological constant. However, these three quantities change their values rapidly as r is increased. This is because the difference of the present metric from the AdS metric is $O(r^3)$ from Eq. (49), and thus, the deviation of the Einstein tensor from the cosmological term is $O(r)$. In this sense, the AdS spacetime does not approximate the spacetime structure around the center of the nonsingular Reissner-Nordström spacetime very well. Around the central region, there appears the region where the NEC and DEC are violated. At the distant place, only the DEC is violated. This can be confirmed to hold for arbitrary M , Q , and ℓ , by the asymptotic expansion,

$$\rho = \frac{Q^2}{r^4} + \frac{12M^2\ell^2}{r^6} + \dots, \quad (57a)$$

$$p_\theta = \frac{Q^2}{r^4} + \frac{24M^2\ell^2}{r^6} + \dots. \quad (57b)$$

3.4. Regularization of ingoing charged Vaidya spacetime

We now describe the methods of regularizing ingoing charged Vaidya spacetime that will be used in the subsequent sections.

3.4.1. Constant regularization. The natural choice of the metric for the regularized ingoing charged Vaidya solution would be to adopt the metric of Eq. (1) with the regularized

function $F_-(v, r)$, which has the same formula as Eq. (48),

$$F_-(v, r) = 1 - \frac{(2M(v)r - Q(v)^2)r^2}{r^4 + (2M(v)r + Q(v)^2)\ell^2}, \quad (58)$$

except that the mass $M(v)$ and the charge $Q(v)$ are now dependent on the advanced time. Here, we introduced a constant ℓ with the dimension of length that determines the scale of the regularization. This is a natural extension of the model by Hayward and Frolov. The property of the spacetime with this choice of $F_-(v, r)$ will be analyzed in Sect. 5. The geometrical properties, such as Riemann invariants and the Einstein tensor, are examined in Appendix D.

3.4.2. Time-dependent regularization. We would like to consider a different choice where the scale of the regularization ℓ depends on the advanced time as

$$\ell(v) = M(v)b, \quad (59)$$

where b is a nondimensional constant. Then, the function $F_-(v, r)$ is

$$F_-(v, r) = 1 - \frac{(2M(v)r - Q(v)^2)r^2}{r^4 + (2M(v)r + Q(v)^2)M(v)^2b^2}. \quad (60)$$

The reason for considering the time-dependent regularization is that the self-similar property of the evaporation model (A), reviewed in Sect. 2.2, is kept for the value of $b \neq 0$ as well, and thus, the analysis can be carried out with a straightforward modification to Sect. 2.2. We present this analysis in the next section. Examinations of geometrical properties in the constant regularization are done in Appendix D.

4. Self-similar model of evaporation

In this section, we study the self-similar model of an evaporating nonsingular charged black hole given by the time-dependent regularization of Eq. (60). The setup is the same as that of the model (A) of an evaporating charged black hole reviewed in Sect. 2.2 except that the time-dependent regularized function $F_-(v, r)$, Eq. (60), is used here. In the domain $0 \leq v \leq v_f$, the functions $M(v)$ and $Q(v)$ are assumed to be the same as Eqs. (14) and (15). In what follows, we briefly describe the results focusing attention to the difference from the model (A) of Sect. 2.2 in the evaporation phase. See also Appendix C for the study on the collapsing phase.

We introduce the two new coordinates \tilde{v} and R by Eq. (16), and then, the function $F_-(v, r)$ of Eq. (60) is rewritten as

$$F_-(v, r) = 1 - \frac{2R^3 - q^2R^2}{R^4 + 2Rb^2 + q^2b^2} =: f(R). \quad (61)$$

In these coordinates, the metric is expressed by the same formula as Eq. (18). The retarded time u can be introduced by Eq. (20), and the metric is expressed as Eq. (21) in the double null coordinates (u, \tilde{v}) .

Similarly to the model (A) of Sect. 2.2, zeros of the function $f\alpha + 2R$ play important roles to determine the spacetime structure. Equation (22) is modified as

$$-\frac{1}{\alpha} = \frac{R^4 - 2R^3 + q^2R^2 + 2Rb^2 + q^2b^2}{2R(R^4 + 2Rb^2 + q^2b^2)} =: y(R). \quad (62)$$

Compared to the $b = 0$ case, the divergence of $y(R)$ in the neighborhood of $R = 0$ becomes weaker. Except that point, the gross behavior of the function $y(R)$ does not change as long

as b is small: The function $y(R)$ has the local minimum and local maximum at $R = R_{\pm}$ in the domain $R > 0$, respectively, and there is zero, one, and two positive solutions in the cases that $1/\alpha > |y(R_-)|$, $1/\alpha = |y(R_-)|$, and $1/\alpha < |y(R_-)|$, respectively. If the equation $f\alpha + 2R = 0$ has only zero positive solution, the spacetime possesses no homothetic Killing horizon except for $\tilde{v} = 0$. On the other hand, if the equation $f\alpha + 2R = 0$ has two positive roots, R_C^- and R_C^+ , they correspond to the homothetic Killing horizons.

The outgoing null coordinate u can be introduced by the same formula as Eq. (20). When the equation $f\alpha + 2R = 0$ has only one (negative) solution, the coordinate u spans the whole domain of $0 \leq R < \infty$, although the explicit integration of Eq. (20) may be difficult. When the equation $f\alpha + 2R = 0$ has two positive solutions, the function $f\alpha + 2R$ can be formally written as

$$f\alpha + 2R = \frac{(R - R_C^-)(R - R_C^+)}{2(R_C^+ - R_C^-)}\kappa(R), \quad (63)$$

where $\kappa(R)$ is some positive regular function of R in the range $0 \leq R < \infty$. Then, the formal integration of Eq. (20) can be performed to give the modified equation of Eq. (24) as

$$u = \ln \tilde{v} - \frac{1}{\kappa_-} \ln |R - R_C^-| + \frac{1}{\kappa_+} \ln |R - R_C^+| + G(R), \quad (64)$$

where $\kappa_{\pm} := \kappa(R_C^{\pm})$ and

$$G(R) := \int \left[\frac{1/\kappa(R) - 1/\kappa_+}{R - R_C^+} - \frac{1/\kappa(R) - 1/\kappa_-}{R - R_C^-} \right] dR. \quad (65)$$

Note that the integrand of $G(R)$ is regular at $R = R_C^{\pm}$. The null coordinates U_{\pm} that are continuous across $R = R_C^{\pm}$ are introduced locally by Eqs. (26), and in these coordinates the metric takes the regular form,

$$ds^2 = - \frac{M_0^2 \alpha \tilde{v}^{1 \mp \kappa_{\pm}} \kappa(R) \exp[\mp \kappa_{\pm} G(R)] |R - R_C^{\mp}|^{1 + \kappa_{\pm}/\kappa_{\mp}}}{2\kappa_{\pm}(R_C^+ - R_C^-)} dU_{\pm} d\tilde{v}. \quad (66)$$

Here, we discuss whether there exist spacetime singularities in this model. The formulas of geometric quantities in this model are presented in Appendix D, and the scalar quantities constructed from the Riemann tensor $\mathcal{R}_{\mu\nu\rho\sigma}$ behave as

$$\mathcal{R}|_{R=0} = - \frac{12}{(bM(v))^2}, \quad (67a)$$

$$\mathcal{R}_{\mu\nu}\mathcal{R}^{\mu\nu}|_{R=0} = \frac{36}{(bM(v))^4}, \quad (67b)$$

$$\mathcal{R}_{\mu\nu\rho\sigma}\mathcal{R}^{\mu\nu\rho\sigma}|_{R=0} = \frac{24}{(bM(v))^4}. \quad (67c)$$

Although the spacetime curvature is finite at $R = 0$ for the region where $M(v) > 0$, it diverges in the limit $M(v) \rightarrow 0$ for $R = 0$ (this statement holds for any fixed R , see Appendix D). Hence, the regularization of the spacetime curvature by the formula of Eq. (60) is not very complete. For this reason, we call this model the partly regularized ingoing charged Vaidya spacetime.

Figure 9 shows the (v, r) -diagrams in the partly regularized case with $b = 0.1$ for $q = 0.7$ (left panel) and $q = 0.9$ (right panel). Similarly to Fig. 3 in the unregularized case with $b = 0$, the behavior of outgoing null geodesics (thin green curves) and the boundary of the

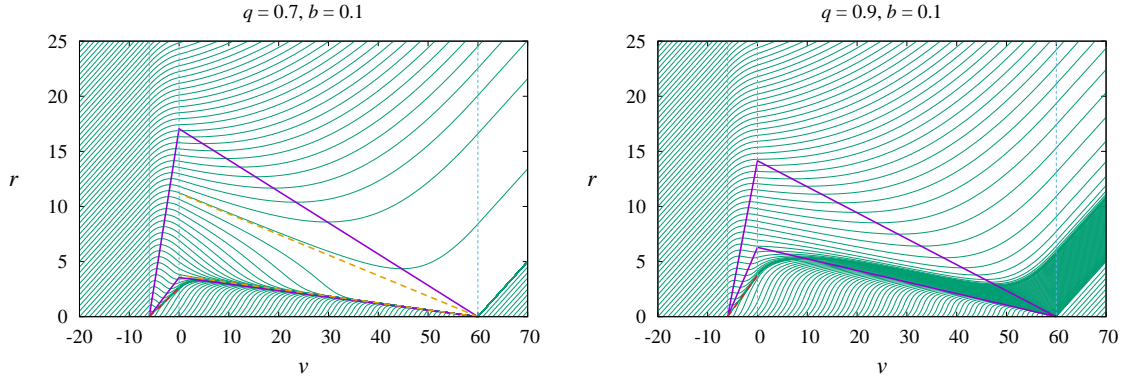


Fig. 9 The same as Fig. 3 but for the partly regularized case of $b = 0.1$.

trapped region (closed purple lines) are shown by selecting the same parameter values of M_0 , v_i , and v_f . The main difference from the $b = 0$ case is the behavior of outgoing null geodesics around $r = 0$ in the range $-v_i < v < v_f$. In the unregularized case, the value of dr/dv diverges because $r = 0$ is a curvature singularity, while in the case $b = 0.1$, we have the value $dr/dv = 1/2$ because the geometry around $r = 0$ is regular. Except that, these (v, r) -diagrams are similar to those of Fig. 3. In the case of $q = 0.7$, there are two homothetic Killing horizons in the evaporating phase as shown by the orange dashed lines. The outer and inner homothetic Killing horizons are the repeller and attractor of outgoing null geodesics. All outgoing null geodesics within the outer homothetic Killing horizon plunge into the curvature singularity at $(v, r) = (v_f, 0)$. This means that the singularity is extended into u direction, and thus, it is a null singularity. The outer homothetic Killing horizon plays the role of the event horizon simultaneously. In the case of $q = 0.9$, no homothetic Killing horizon is present in the evaporating phase, and thus, there is no event horizon. The singularity at $(v, r) = (v_f, 0)$ is not extended in the u direction because no outgoing null geodesic plunges into this singularity from $v < v_f$. In the collapsing phase, there is one homothetic Killing horizon as indicated by the red dashed line in both cases of $q = 0.7$ and 0.9 . Since this homothetic Killing horizon is the attractor of outgoing null geodesics in the future direction, only one outgoing null geodesic is emitted from the singularity at $(v, r) = (-v_i, 0)$. This means that this singularity is not extended in the u direction and is a pointlike singularity.

We now present the Penrose diagram for the evaporation of a partly regularized Reissner-Nordström black hole in the self-similar model, which corresponds to the right panel of Fig. 9. The left panel of Fig. 10 shows the Penrose diagram for the case that no homothetic Killing horizon exists in the evaporating phase. Compared to the corresponding diagram of Fig. 4(b) of Sect. 2.2, the timelike singularity at $R = 0$ (hence, $r = 0$) is regularized. However, the pointlike singularity appears at $r = \tilde{v} = 0$ due to Eqs. (67a)–(67c), and a Cauchy horizon is formed on the future light cone of $r = \tilde{v} = 0$. Except for this feature, the Penrose diagram possesses good properties for solving the information loss problem since the diagram is similar to that of the Minkowski spacetime.

Right panel of Fig. 10 shows the Penrose diagram for the case that two homothetic Killing horizons exist in the evaporating phase, which corresponds to the left panel of Fig. 9. Compared to the corresponding diagram of Fig. 5(b) of Sect. 2.2, the timelike singularity at $R = 0$

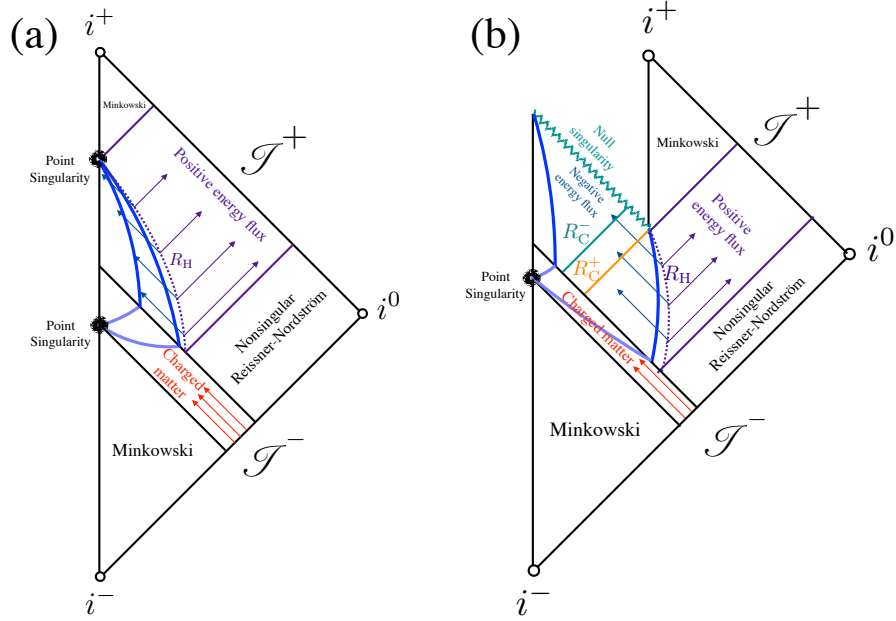


Fig. 10 Penrose diagram for evaporation of a partly regularized Reissner-Nordström black hole. Left panel: The case that a homothetic Killing horizon does not exist. A pointlike singularity forms. Right panel: The case that two homothetic Killing horizons exist. There appears a null singularity inside the invisible region.

is regularized in the domain $\tilde{v} > 0$. However, the null singularity still remains at $\tilde{v} = 0$ and $R = R_C^-$ because of Eqs. (67a)–(67c). As a result, the domain $0 < R < R_C^+$ is invisible to outside observers. This property is not good for solving the information loss problem because the information of the invisible domain will be lost in the process of evaporation.

To summarize, the spacetime structures of the partly regularized evaporating Reissner-Nordström black holes do not have satisfactory features for solving the information loss problem. However, we do not consider that the Hayward-Frolov scenario fails because of this result. Rather, the time-dependent regularization introduced in Sect. 3.4.2 would not be appropriate. In fact, the motivation for introducing time-dependent regularization was that the self-similarity of the spacetime is maintained and the analytic method of Kaminaga [26] can be extended straightforwardly. The appropriate interpretation of this result is that the constant regularization of Sect. 3.4.1 would be a more preferred one. In the next section, we study the global structure of an evaporating charged black hole applying the constant regularization.

5. Model of evaporation with regularized center: Non-self-similar case

We now consider the constant regularization, where the function $F_-(v, r)$ is given by Eq. (58). In Sect. 5.1, we adopt the linear mass function of Eq. (14) and compare the case $\ell = 0$ (Kaminaga’s model) and the case $\ell \neq 0$ (the nonsingular model). In Sect. 5.2, we study the case of the nonlinear mass function, and present the Penrose diagram. Section 5.3 is devoted to the numerical study on the frequency shift of a photon that falls into the black hole and comes out of it at the last stage of the evaporation.

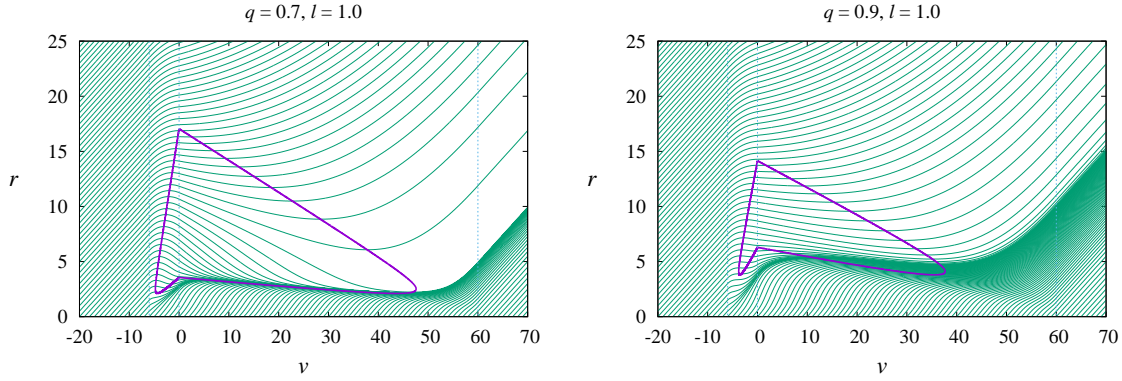


Fig. 11 The same as Fig. 3 and Fig. 9 but for the completely regularized case of $\ell = 1.0$.

5.1. The case of the linear mass function and comparison with Kaminaga's model

In this section, we compare the case of the constant regularization with the unregularized case (Kaminaga's self-similar spacetime). This helps us to understand how the constant regularization works in the Hayward-Frolov model. Except for the value of ℓ , we choose the same setups: The linear mass function of Eq. (14) and the same parameters, $M_0 = 10$, $v_i = 6$, and $v_f = 60$, as those of Fig. 3, are adopted. The values of q of Eq. (15) is assumed to be constant, and the cases $q = 0.7$ and 0.9 are discussed.

Figure 11 shows the (v, r) -diagrams for $q = 0.7$ (left panel) and 0.9 (right panel) for the case $\ell = 1.0$. Let us discuss the case of $q = 0.7$ first. In the unregularized case ($\ell = 0$), the left panel of Fig. 3 shows that there exist two homothetic Killing horizons and all outgoing null geodesics within the outer homothetic Killing horizon are trapped and plunge into the singularity at $(v, r) = (v_f, 0)$. By contrast, in the regularized case (left panel of Fig. 11), the self-similar structure is broken by the introduction of nonzero ℓ , and all of the null geodesics escape to infinity. Furthermore, the regularization of the spacetime is complete and no singularity appears. Therefore, the spacetime possesses the desired property of the Hayward-Frolov scenario: the event and Cauchy horizons are not present. Although the spacetime structure drastically changes from the unregularized case, the behavior of the null geodesics at distant positions from the center is similar to the case $\ell = 0$. The homothetic Killing horizons are absent, but we can recognize the existence of the temporal repeller and attractor for a certain range of v . The boundary of the trapped region is topologically closed, and it is called the closed apparent horizon in Ref. [10]. The temporal attractor is located in the neighborhood of the inner boundary of the trapped region. These repeller and attractor would be a kind of residues of the homothetic Killing horizons.

Next we discuss the case $q = 0.9$. In the case of $\ell = 0$ (the right panel of Fig. 3), the homothetic Killing horizons do not exist and all outgoing null geodesics escape to infinity. The behavior of outgoing null geodesics in the regularized spacetime of the right panel of Fig. 11 is similar to the unregularized case except that the singularity is completely resolved. Reflecting the absence of the homothetic Killing horizon in the case $\ell = 0$, the temporary repeller and attractor are not found. Similarly to the left panel, no event horizon or no Cauchy horizon is present, and the Hayward-Frolov scenario works well also for $q = 0.9$.

To summarize, by introducing the constant regularization scale ℓ , the singularity completely vanishes, while the temporal repeller and attractor are present for certain range of v for small q . The absence of the temporary repeller/attractor for a large q in the regularized spacetime is understood from the absence of the homothetic Killing horizons in the unregularized case. We do not present the Penrose diagrams for Fig. 11 here, because they are similar to the one that will be drawn in a slightly different setup below.

5.2. The case of the nonlinear mass function

Since there cannot exist a self-similar configuration in the case that $\ell \neq 0$, it is not necessary to stick to the linear mass function of Eq. (14). Below, we study the case that the mass function is assumed as

$$M(v) = \begin{cases} 0 & (v \leq -v_i), \\ M_0 (1 + v/v_i) & (-v_i \leq v \leq 0), \\ M_0 (1 - v/v_f)^{1/3} & (0 \leq v \leq v_f), \\ 0 & (v \geq v_f). \end{cases} \quad (68)$$

In this case, the time evolution of the mass in the evaporation period, $0 \leq v \leq v_f$, is expected to resemble that of the realistic Hawking evaporation. The setup here is similar to that of Frolov [10], and we can observe how the electric charge affects the spacetime structure in the Hayward-Frolov scenario. As for the charge function, we adopt Eq. (15) with a constant q for simplicity. Note that in a realistic evaporation, the black hole does not conserve the ratio of the electric charge to the mass, and the value of q in Eq. (15) depends on time in general [40–42]. A more detailed study on this scenario with a more realistic evolution of the charge function is left for future study.

Below, we draw the Penrose diagram of the regularized ingoing charged Vaidya spacetime in this setup. For constructing the model of an evaporating black hole, we have to cut the appropriate domain out, and glue the regularized Reissner-Nordström spacetime and the regularized outgoing charged Vaidya spacetime. This method is discussed in Appendix E.

5.2.1. Method of drawing Penrose diagram. The numerical calculation of the outgoing null geodesics is performed in the same way as explained in Sect. 2.2.5. Each geodesic can be regarded as a surface of the constant advanced time u . The value of u is naturally assigned by requiring

$$u = v - 2r \quad (69)$$

in the Minkowski domain $v_f < v$ after the evaporation. Once the u coordinate is generated, we specify the locations of the central point $r = 0$ and of the boundary of the trapped region at which $F_-(v, r) = 0$ in the (u, v) -plane.

In order to show the spacetime in a compact domain, two compact coordinates (η, ζ) are introduced as

$$\eta = \arctan(v/L) + \arctan(u/L), \quad (70a)$$

$$\zeta = \arctan(v/L) - \arctan(u/L), \quad (70b)$$

where L is a positive constant with the dimension of length whose value can be arbitrarily chosen. In these coordinates, whole spacetime is shown within the diamond-shaped domain, $-\pi < \eta \pm \zeta < \pi$.

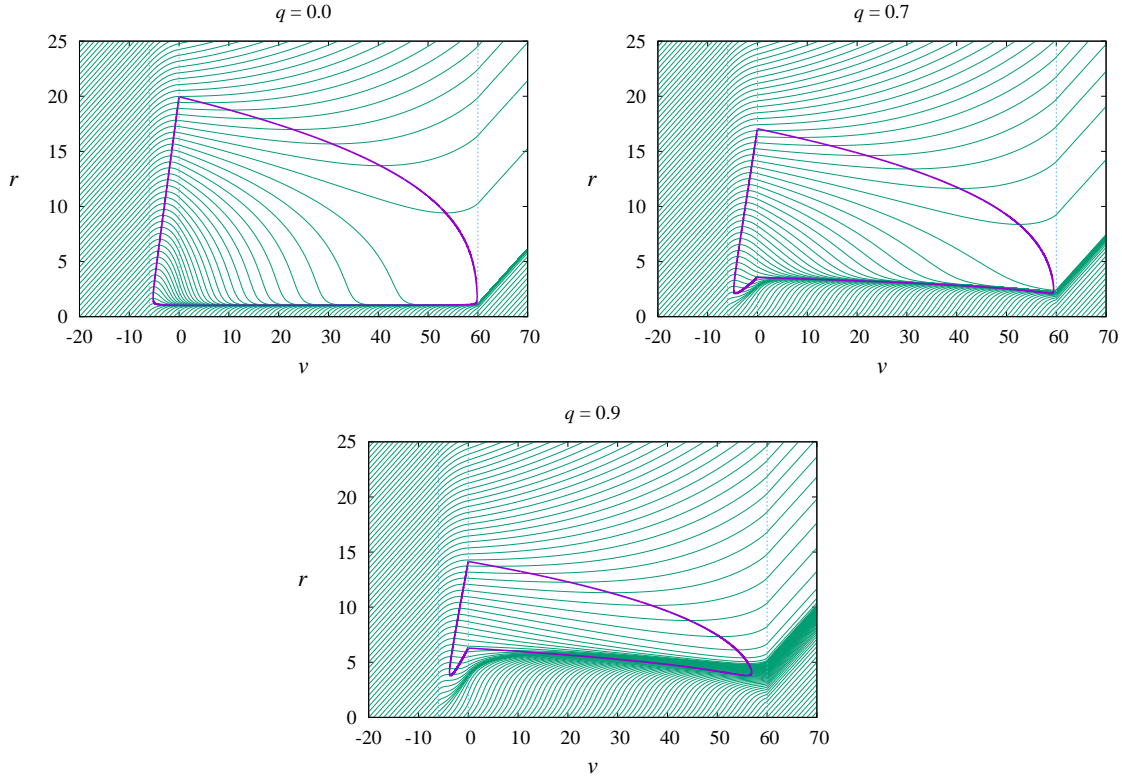


Fig. 12 Outgoing null geodesics (thin green curves) and the boundary of the trapped region (closed purple curve) for $q = 0.0$ (upper left panel), 0.7 (upper right panel), and 0.9 (lower panel) for the nonlinear mass function of Eq. (68). The vertical dotted lines in each panel indicate $v = -v_i$, 0 , and v_f from left to right. The unit of the length is ℓ .

5.2.2. Outgoing null geodesics and the Penrose diagram. We now show the results for the nonlinear mass function given by Eq. (68). We select the same parameters as Sect. 5.1, i.e., $M_0/\ell = 10$, $v_i/\ell = 6$, and $v_f/\ell = 60$ as an example. Figure 12 shows the (v, r) -diagrams for $q = 0.0$ (upper left), 0.7 (upper right), and 0.9 (bottom). Each of the outgoing null geodesics gives a u -constant surface. In all cases, all outgoing null geodesics escape to future null infinity, similarly to the case of the linear mass function of Sect. 5.1.

In each figure for $q = 0.0$ and $q = 0.7$, we can observe the existence of an attractor near the inner boundary of the trapped region which attracts outgoing null geodesics for some period of time. In the case of $q = 0.0$, the radial position of the attractor is approximately constant. This is because the geometry near the center is approximately equal to that of the dS spacetime, and the attractor is understood as the cosmological horizon in that geometry. On the other hand, for $q = 0.7$, the geometry around the center is similar to that of the AdS spacetime (see Appendix D). In that case, there is no cosmological horizon and the reason for the existence of the attractor is different from the case $q = 0.0$. It would be understood by the similarity to the case of the linear mass function, i.e., as the residue of the inner homothetic Killing horizons of the case $\ell = 0$ (compare with the right panel of Fig. 11). Although the gathering of outgoing null geodesics also occurs for $q = 0.9$, the attractive property does not seem to be sufficiently strong to form an attractor. This result is also similar to the case of

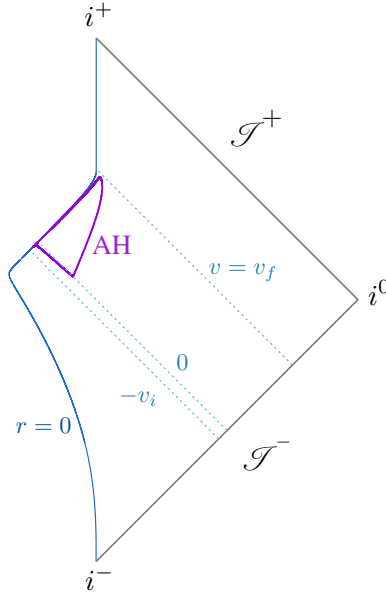


Fig. 13 Penrose diagram of the collapse of a charged null fluid and the subsequent evaporation in the case that the mass function $M(v)$ is chosen as Eq. (68) for the parameters $q = 0.9$, $M_0/\ell = 10$, $v_i/\ell = 6$, and $v_f/\ell = 60$.

the linear mass function (compare with the right panel of Fig. 11). In all cases, the gathering of outgoing null geodesics causes the blueshift of propagating photons. This frequency shift will be studied in more detail in Sect. 5.3.

We now show the Penrose diagram for $q = 0.9$ in Fig. 13. This diagram is drawn with the value $L = v_f = 60\ell$ in Eqs. (70a) and (70b). The blue curve shows the worldline of the central point, $r = 0$, and the purple curve shows the closed apparent horizon. In this spacetime, there is no event horizon because the past of the future null infinity covers all spacetime regions. Also, no singularity formation happens, and hence, there is no Cauchy horizon either. The Penrose diagram has the same structure as that of the Minkowski spacetime, and therefore, no information problem occurs in this spacetime. Thus, we have obtained the result that is consistent with the Hayward-Frolov scenario.

In this diagram, the inner boundary of the trapped region and the worldline of $r = 0$ almost degenerate. This is because some of the outgoing null geodesics tend to gather around the inner boundary of the trapped region, and such outgoing geodesics have similar u values. In Appendix F, we present a Penrose diagram for the same spacetime drawn in a different way. There, the inner boundary of the trapped region and the worldline of $r = 0$ are clearly separated.

5.3. Frequency shift

Since the spacetime possesses no event and Cauchy horizons, a photon that falls into the black hole will come out from it eventually. Frolov pointed out that some of them are highly blueshifted in the uncharged case [10]. In that paper, the blueshift experienced by a photon propagating along the attractor was calculated analytically. In the charged case, it is difficult to estimate the strength of the blueshift analytically because the attractive property becomes

vague for q close to unity. For this reason, we perform numerical calculations in the setup of Sect. 5.2 as follows.

We consider only photons with zero angular momenta, and suppose that a photon is incident from past null infinity along $v = v_{\text{in}}$. The angular frequency for the observers staying at constant spatial coordinates (for large r) is denoted by ω_{in} . Then, the photon comes out along $u = u_{\text{out}}$, and at the distant place, the same observers measure its angular frequency ω_{out} . We compute the ratio of the two angular frequencies, $\omega_{\text{out}}/\omega_{\text{in}}$. If this quantity is smaller/greater than unity, the outcoming photon is redshifted/blueshifted.

We derive the necessary formula for computing this quantity. Hereafter, the affine parameter of a null geodesic is denoted as λ and dot indicates the derivative with respect to λ . The tangent vector to the null geodesic is $k^\mu = (\dot{v}, \dot{r}, 0, 0)$, and the geodesic equations are

$$\ddot{r} - F_- \ddot{v} - \frac{1}{2} F_{-,v} \dot{v}^2 - F_{-,r} \dot{r} \dot{v} = 0, \quad (71a)$$

$$\ddot{v} + \frac{1}{2} F_{-,r} \dot{v}^2 = 0. \quad (71b)$$

From the null condition, we have $\dot{v} = 0$ for an ingoing photon and $F_-(v, r) \dot{v} = 2\dot{r}$ for an outcoming photon. The four-velocity of the observers staying at constant r, θ, ϕ coordinates is

$$u_{(o)}^\mu = \left(\frac{1}{\sqrt{F_-}}, 0, 0, 0 \right), \quad (72)$$

and the angular frequency of a photon for these observers is

$$\omega = -k_\mu u_{(o)}^\mu = \sqrt{F_-} \dot{v} - \frac{1}{\sqrt{F_-}} \dot{r}. \quad (73)$$

First, we consider the incident photon with $\dot{v} = 0$. For the observer at distant position ($r \rightarrow \infty$), the observed angular frequency is $\omega_{\text{in}} = -\dot{r}|_{r=\infty}$ since $F_- = 1$ holds at $r \rightarrow \infty$. We introduce an auxiliary observer staying at the center, $r = 0$. The angular frequency observed by this auxiliary observer is $\omega_c = -\dot{r}|_{r=0}$ since $F_- = 1$ also holds at $r = 0$. Since Eq. (71a) indicates $\ddot{r} = 0$ for $\dot{v} = 0$, we have $\dot{r} = \text{constant}$. Therefore, $\omega_{\text{in}} = \omega_c$ is obtained.

Next, we consider the outcoming photon with $F_-(v, r) \dot{v} = 2\dot{r}$. The angular frequencies observed by the auxiliary observer at the center $r = 0$ and the distant observer at $r \rightarrow \infty$ is $\omega_c = (1/2) \dot{v}|_{r=0}$ and $\omega_{\text{out}} = (1/2) \dot{v}|_{r=\infty}$, respectively. Therefore, we have

$$\frac{\omega_{\text{out}}}{\omega_{\text{in}}} = \frac{\omega_{\text{out}}}{\omega_c} = \frac{\dot{v}|_{r=\infty}}{\dot{v}|_{r=0}}. \quad (74)$$

In order to evaluate this quantity, we divide both sides of Eq. (71b) with \dot{v} and integrate them from $\lambda = 0$ to ∞ , where $\lambda = 0$ is the affine parameter at the center, $r = 0$. The result is

$$\frac{\omega_{\text{out}}}{\omega_{\text{in}}} = \exp \left[-\frac{1}{2} \int_{v_{\text{in}}}^{v_{\text{f}}} F_{-,r}(v, r(v)) dv \right], \quad (75)$$

where we used $F_- = 1$ for $v \geq v_{\text{f}}$. After obtaining the numerical data of outgoing null geodesics, $r(v)$, numerical integrations of this formula can be computed easily.

Figure 14 shows the behavior of $\omega_{\text{out}}/\omega_{\text{in}}$ in the logarithmic scale for the case $q = 0.0, 0.7$, and 0.9 . Since each geodesic has the values of v_{in} and u_{out} , the quantity $\omega_{\text{out}}/\omega_{\text{in}}$ is shown as functions of v_{in} and u_{out} in the left and right panels, respectively. In all cases, the redshift

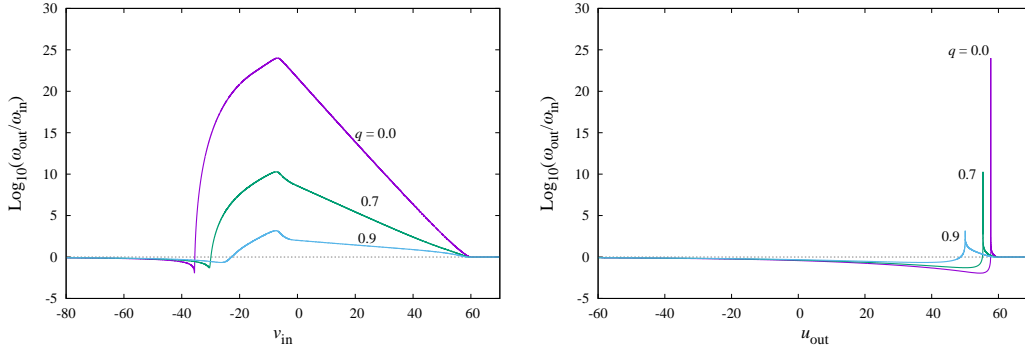


Fig. 14 The factor $\omega_{\text{out}}/\omega_{\text{in}}$ as a function of v_{in} (left panel) and of u_{out} (right panel) in the cases of $q = 0.0, 0.7$, and 0.9 . The unit of the horizontal axis is ℓ .

happens initially, and the blueshift occurs after that. If $\omega_{\text{out}}/\omega_{\text{in}}$ is regarded as a function of u_{out} , the curve for $q = 0$ has a sharp peak with an extremely large peak value, while the duration of the blueshift is very short. As the value of q is increased, the peak becomes less sharp, and the duration becomes longer instead. This reflects the fact that the attractive property around the inner boundary of the trapped region becomes weaker for larger q .

This blueshift at the last stage of evaporation may lead to interesting astrophysical phenomena. Also, it would be interesting to study the property of Hawking radiation caused by this blueshift, as pointed out in [10] and analyzed in [16, 17] in the uncharged case. These issues are left as remaining problems to be discussed in future.

6. Summary and discussion

In this paper, we have studied the collapse of a charged matter and its evaporation in the situation that the central singularity is resolved, in order to assess whether the Hayward-Frolov scenario possesses sufficient generality. In Sect. 3, we have constructed the simplest model of the (static) regularized Reissner-Nordström black hole spacetime and the regularized charged Vaidya spacetime. The spacetime structure of an evaporating black hole has been studied using two kinds of regularization, the time-dependent regularization and the constant regularization, in Sects. 4 and 5, respectively. The time-dependent regularization, where the regularization scale is proportional to mass as $\ell(v) = bM(v)$, has been considered since the spacetime possesses the self-similarity and analytical construction of double null coordinates is possible if we choose a linearly decreasing mass function $M(v)$. The result is that a point singularity or a null singularity is formed in this spacetime, and the resolution is not sufficient to resolve the information loss problem. In the study of the constant regularization, where the scale of the regularization ℓ is fixed, we have obtained the Penrose diagrams of Fig. 13. The resultant spacetime possesses no event horizon, no singularity, and no Cauchy horizon, and therefore, the information loss problem does not arise. This result supports the Hayward-Frolov scenario.

We have also examined the properties of both Kaminaga's model and the evaporating non-singular Reissner-Nordström black hole and compared the two results. In the case of Kaminaga's model, the inner and outer homothetic Killing horizons exist for the case of a sufficiently small charge, and they coincide with the attractor and repeller of outgoing null

geodesics. For the case that the charge is sufficiently large, there is no such an attractor or a repeller because the homothetic Killing horizons are absent. A similar phenomena could be observed in the nonsingular model. Although an attractor and a repeller can be temporally found in the case of a small charge, both of them vanish for the case of a sufficiently large charge. Reflecting the absence of the attractor, the blueshift of outgoing photons at the last stage of the evaporation becomes weaker as the charge is increased. Correspondingly, the period during which the blueshift can be observed becomes longer for outside observers.

There remains several issues to be explored. First, as mentioned in Sect. 1, Levin and Ori [27] suggested that there are two possible cases for the models of collapse of charged null matter and its evaporation, which they called models (A) and (B). The model (A) corresponds to Kaminaga's model in which the accreting matter continues to implode to the center. On the other hand, in the model (B), the accreting charged null matter experiences bounce at some radius. Although both models are the solution to Einstein's equations, it was suggested that the model (B) would be more plausible. Regularizing such a spacetime would be more difficult than the analysis of the present paper, and we postpone this problem for the future work.

Second, whether the Hayward-Frolov model holds for systems with angular momenta must be investigated. Since the Penrose diagram of a Kerr black hole is very similar to the diagram of the Reissner-Nordström black hole, we expect that the information loss problem would be solved for the system with angular momentum in a similar manner. The explicit construction of the model for the gravitational collapse of a rotating star and its evaporation is necessary for clarifying this point. The Kerr-Vaidya solution [44] may be useful for this purpose.

Third, the mechanism of regularizing the curvature singularity must be studied. As cited in Sect. 1, there are several existing works that realize the spacetime of an evaporating black hole without curvature singularity [11–15, 18–21]. In addition to these works, a new mechanism to resolve the curvature singularity due to running of the gravitational constant is proposed recently [43]. It would be interesting to examine whether this mechanism realizes the Hayward-Frolov scenario.

Finally, we have to comment on the existing works [45] (see also [46]) that raised doubts for the Hayward-Frolov scenario. If the evaporation of a black hole with the metric of Eqs. (35) and (36) is considered in the quasistatic approximation, the two horizons tend to degenerate as the mass is decreased in the evaporation. Then, the temperature of the black hole becomes zero, the Hawking radiation stops, and a remnant remains. Inside of the remnant, the Cauchy horizon is formed and the instability develops around it. If this is the case, the Hayward-Frolov scenario would not work well to resolve the information loss problem.

Our opinion on this issue is as follows. Recall that the black hole is supposed to evaporate completely within a finite time in the works of Hayward and Frolov. In such a case, both the event and Cauchy horizons do not appear in the spacetime. The same thing has happened in the analysis of our paper. In Sect. 1, we asked whether the singularity that develops near the Cauchy horizon must be resolved in the system with electric charge/angular momentum, and our analysis indicates that such a procedure is not necessary. This is because the development of the Cauchy horizon is a phenomena associated with infinite time (with respect to the outside domain of the black hole), while the black hole is assumed to evaporate in a finite time in our model. In the analyses Hayward, Frolov, and us, the quasi-static approximation is obviously violated at the last stage of the evaporation as indicated by the disappearance

of the trapped region. In this sense, the Hayward-Frolov scenario requires the violation of quasistatic approximation.

From this observation, it is very important to determine whether the regularized black hole evaporates completely in a finite time or not. For this purpose, a more refined model of the evaporation process must be developed by taking account of the backreaction effects of the Hawking radiation. We hope to clarify this problem in near future.

Acknowledgements

The authors thank Ken-ichi Nakao and Hideki Maeda for helpful comments and discussions. K.S. is in part, supported by Japan Science and Technology Agency, the establishment of university fellowships towards the creation of science technology innovation, Grant Number JPMJFS2138. H. Y. is in part supported by JSPS KAKENHI Grant Numbers JP22H01220 and JP21H05189, and is partly supported by Osaka Central Advanced Mathematical Institute (MEXT Joint Usage/Research Center on Mathematics and Theoretical Physics JPMXP0619217849).

A. Homothetic Killing vector field of the self-similar model

In this Appendix, we present the detailed calculations that show the presence of a homothetic Killing vector field for the self-similar model of an evaporating charged black hole in Sects. 2.2 and 4.

For simplicity, we express the metric as $ds^2 = -A(u, \tilde{v})du d\tilde{v} + r(u, \tilde{v})^2 d\Omega^2$, where

$$A(u, \tilde{v}) = M_0^2 \alpha \tilde{v} (f\alpha + 2R). \quad (\text{A1})$$

We write the covariant components of the homothetic Killing vector as

$$\xi_\mu = (\xi_u, \xi_{\tilde{v}}, 0, 0). \quad (\text{A2})$$

The (u, u) and (\tilde{v}, \tilde{v}) components of the homothetic Killing equation, Eq. (28), are

$$-\frac{2\xi_u \partial_u A}{A} + 2\partial_u \xi_u = 0, \quad (\text{A3a})$$

$$-\frac{2\xi_{\tilde{v}} \partial_{\tilde{v}} A}{A} + 2\partial_{\tilde{v}} \xi_{\tilde{v}} = 0, \quad (\text{A3b})$$

respectively, and these equations are integrated as

$$\xi_u(u, \tilde{v}) = C_u(\tilde{v})A(u, \tilde{v}), \quad (\text{A4a})$$

$$\xi_{\tilde{v}}(u, \tilde{v}) = C_{\tilde{v}}(u)A(u, \tilde{v}). \quad (\text{A4b})$$

Substituting these formulas into the (u, \tilde{v}) and (θ, θ) components of the homothetic Killing equation, we have

$$\frac{dC_u}{d\tilde{v}} + \frac{dC_{\tilde{v}}}{du} + \frac{1}{A} \frac{\partial A}{\partial \tilde{v}} C_u + \frac{1}{A} \frac{\partial A}{\partial u} C_{\tilde{v}} = -\frac{K}{2}, \quad (\text{A5})$$

$$\frac{1}{r} \partial_v r C_u + \frac{1}{r} \partial_u r C_{\tilde{v}} = -\frac{K}{4}, \quad (\text{A6})$$

respectively. Note that the (ϕ, ϕ) component is the same as the (θ, θ) component due to spherical symmetry. Eliminating K from these equations, we obtain

$$\frac{dC_u}{d\tilde{v}} + \left(\frac{1}{A} \frac{\partial A}{\partial \tilde{v}} - \frac{2}{r} \frac{\partial r}{\partial \tilde{v}} \right) C_u + \frac{dC_{\tilde{v}}}{du} + \left(\frac{1}{A} \frac{\partial A}{\partial u} - \frac{2}{r} \frac{\partial r}{\partial u} \right) C_{\tilde{v}} = 0. \quad (\text{A7})$$

Here, we rewrite the formulas in the parentheses in this equation using Eqs. (A1) and (20). The result is

$$\frac{dC_u}{d\tilde{v}} + \frac{\alpha}{\tilde{v}} \left(\frac{f}{R} - \frac{1}{2} \frac{df}{dR} \right) C_u + \frac{dC_{\tilde{v}}}{du} + \left(-1 + \frac{\alpha}{2} \frac{df}{dR} - \frac{f\alpha}{R} \right) C_{\tilde{v}} = 0. \quad (\text{A8})$$

Putting $C_u(\tilde{v}) = \tilde{v}\tilde{C}_u(\tilde{v})$, this equation becomes

$$\left(\tilde{v} \frac{d\tilde{C}_u}{d\tilde{v}} + \frac{dC_v}{du} \right) + \left[1 + \alpha \left(\frac{f}{R} - \frac{1}{2} \frac{df}{dR} \right) \right] (\tilde{C}_u - C_v) = 0. \quad (\text{A9})$$

It follows that $C_v = \tilde{C}_u = \text{constant}$ is the solution to this equation. With a constant parameter χ , the covariant and contravariant components of the homothetic Killing vector field in this spacetime is

$$\xi_\mu = \chi A(u, \tilde{v})(\tilde{v}, 1, 0, 0), \quad (\text{A10a})$$

$$\xi^\mu = -2\chi(1, \tilde{v}, 0, 0). \quad (\text{A10b})$$

The norm of the homothetic Killing vector is

$$g_{\mu\nu}\xi^\mu\xi^\nu = -4\chi^2\tilde{v}A(u, \tilde{v}). \quad (\text{A11})$$

From this result, ξ^μ becomes null at positions satisfying $A(u, \tilde{v}) = 0$, and thus, the homothetic Killing horizons can be found by solving the equation $f\alpha + 2R = 0$. Choosing $\chi = 1/2$, the homothetic Killing vector field becomes $\xi^\mu = -(1, \tilde{v}, 0, 0)$ [that is, Eq. (29)] and satisfies Eq. (28) with $K = -2$.

B. Apparent horizons in Vaidya spacetime

In this Appendix, we show that the boundaries of the trapped region (or the apparent horizon) are located at the radial position satisfying $F_-(v, r) = 0$ in (both regularized and nonregularized) Vaidya spacetimes. The following calculations hold for both charged and uncharged cases.

Let us compute the expansion of the congruence of the outgoing radial null geodesics. Since the null condition $ds^2 = 0$ implies

$$0 = dv(-F_-dv + 2dr), \quad (\text{B1})$$

we have the conditions for the ingoing null geodesics $dv = 0$ and the outgoing null geodesics $F_-dv = 2dr$. This implies that the tangent vector k^μ of the outgoing null geodesics can be expressed as $k^\mu = (1, F_-/2, 0, 0)$ in the (v, r, θ, ϕ) coordinates. The geodesic equation expressed in terms of k^μ is

$$k^\nu \nabla_\nu k^\mu = \kappa k^\mu \quad \text{with} \quad \kappa = \frac{1}{2} \partial_r F_-. \quad (\text{B2})$$

From this formula, $k^\mu = dx^\mu/d\lambda$ is the tangent vector of a geodesic parametrized by a non-affine parameter λ . In terms of the affine parameter λ^* , the tangent vector is expressed as $k_*^\mu = dx^\mu/d\lambda^*$ and satisfies $k_*^\nu \nabla_\nu k_*^\mu = 0$. From a simple calculation, the relation between k_*^μ

and k^μ is shown to be given by

$$k_*^\mu = \exp\left(-\int \kappa d\lambda\right) k^\mu. \quad (\text{B3})$$

Then, the expansion Θ of the null geodesic congruence can be computed as

$$\Theta := \nabla_\mu k_*^\mu = \exp\left(\int \kappa d\lambda\right) \frac{F_-}{r}. \quad (\text{B4})$$

This shows that the contour surfaces of $F_-(v, r) = 0$ are the boundaries of the trapped region, and the outermost one is the apparent horizon.

The interpretation of this result is as follows. The zero expansion of the outgoing null geodesic congruence is realized at a position where the change in the sectional area $4\pi r^2$ along the congruence becomes zero, that is, $dr = 0$. This condition with the null condition $-F_- dv + 2dr = 0$ implies that $F_- = 0$ is the condition for zero expansion.

C. Spacetime structure of the collapse domain

In this Appendix, we present the analysis of the spacetime structure in the collapse domain of a charged null-matter fluid in the self-similar cases of Sects. 2 and 4. We adopt the metric of the ingoing Vaidya metric of Eq. (1), and consider the collapse domain, $-v_i \leq v \leq 0$, of Eqs. (14) and (68). The charge function is related to the mass function as Eq. (15). In the similar manner to the analysis of the evaporation phase, $0 \leq v \leq v_f$, we introduce new coordinates, $\tilde{v} = M(v)/M_0$ and $R = r/M(v)$. Then, for the function $F_-(v, r)$ in the self-similar cases given by Eq. (60), the function can be written in the same form as Eq. (61), i.e. $F_-(v, r) = f(R)$. Introducing $\alpha = v_i/M_0$, the metric is rewritten as

$$ds^2 = -M_0^2 \alpha \tilde{v} (f\alpha - 2R) d\tilde{v} \left(\frac{d\tilde{v}}{\tilde{v}} - \frac{2dR}{f\alpha - 2R} \right). \quad (\text{C1})$$

From this equation, the null coordinate u can be defined as

$$u = \ln \tilde{v} - \int \frac{2dR}{f\alpha - 2R}, \quad (\text{C2})$$

and then, the metric is given as $ds^2 = -M_0^2 \alpha \tilde{v} (f\alpha - 2R) d\tilde{v} du$. Below, we consider the case without regularization (Kaminaga's model in Sect. 2, or equivalently, the case $b = 0$ of Sect. 4) and the case with time-dependent regularization ($b \neq 0$ in Sect. 4), separately.

C.1. The case without regularization

Similarly to the analysis in the evaporation domain of Sect. 2, the homothetic Killing horizons play an important role. As shown in Appendix A, the homothetic Killing horizons exist at positions where $f\alpha - 2R = 0$ is satisfied, and this equation is rewritten as

$$\frac{1}{\alpha} = \frac{R^2 - 2R + q^2}{2R^3} =: y(R). \quad (\text{C3})$$

The definition of $y(R)$ is the same as Eq. (22), and the graph of the function $y(R)$ is shown in Fig. 2 for the case $q = 0.6$. As noted in the main text, $y(R)$ takes extremal values at $R = R_\pm := 2 \pm \sqrt{4 - 3q^2}$, and there, $y(R_-) < 0$ and $y(R_+) > 0$ are satisfied. Since α is a

positive constant, Eq. (C3) has one, two, and three solutions in the cases that $1/\alpha > y(R_+)$, $1/\alpha = y(R_+)$, and $1/\alpha < y(R_+)$, respectively, where

$$y(R_+) = \frac{2 - q^2 + \sqrt{4 - 3q^2}}{(2 + \sqrt{4 - 3q^2})^3}. \quad (\text{C4})$$

Therefore, the mass accretion rate $1/\alpha = M_0/v_i$ and the electric charge per unit mass q determine the number of the homothetic Killing horizons.

We suppose that the mass accretion rate can be controlled and the simple case can be selected. For this reason, the case that $f\alpha - 2R = 0$ has one solution (denoted as $R = R_C$) is considered below. In this case, $f\alpha - 2R$ can be factorized as

$$\begin{aligned} f\alpha - 2R &= -\frac{2}{R^2}(R^3 + \alpha R^2 + 2\alpha R - \alpha q^2) \\ &= -\frac{2}{R^2}(R - R_C)(R^2 + C_1 R + C_2), \end{aligned} \quad (\text{C5})$$

with constants R_C , C_1 , and C_2 satisfying $R_C > 0$ and $C_2 > C_1^2/4$. Then, the integral of Eq. (C2) can be carried out as

$$u = \ln \tilde{v} + \frac{1}{\kappa_A} \arctan \left[\frac{C_1 + 2R}{\sqrt{-C_1^2 + 4C_2}} \right] + \frac{1}{\kappa_B} \ln(R^2 + C_1 R + C_2) + \frac{1}{\kappa_C} \ln |R - R_C|, \quad (\text{C6})$$

with

$$\kappa_A = -\frac{(R_C^2 + C_1 R_C + C_2)\sqrt{-C_1^2 + 4C_2}}{C_1 C_2 + C_1^2 R_C - 2C_2 R_C}, \quad (\text{C7a})$$

$$\kappa_B = \frac{2(R_C^2 + C_1 R_C + C_2)}{C_1 R_C + C_2}, \quad (\text{C7b})$$

$$\kappa_C = \frac{R_C^2 + C_1 R_C + C_2}{R_C^2}. \quad (\text{C7c})$$

The value of u diverges at $R = R_C$, and this coordinate singularity must be resolved. This is done by introducing the new coordinate

$$U = \begin{cases} -\exp(\kappa_C u) & (R > R_C), \\ \exp(\kappa_C u) & (R < R_C), \end{cases} \quad (\text{C8})$$

and then, the relation between U , \tilde{v} and R is given by

$$\frac{U}{\tilde{v}^{\kappa_C}} = -(R - R_C)(R^2 + C_1 R + C_2)^{\frac{\kappa_C}{\kappa_B}} \exp \left(\frac{\kappa_C}{\kappa_A} \arctan \left[\frac{C_1 + 2R}{\sqrt{-C_1^2 + 4C_2}} \right] \right). \quad (\text{C9})$$

Using U , the metric is expressed as

$$ds^2 = -\frac{2\alpha M_0^2}{\kappa_C R^2} \tilde{v}^{1-\kappa_C} (R^2 + C_1 R + C_2)^{1-\frac{\kappa_C}{\kappa_B}} \exp \left(-\frac{\kappa_C}{\kappa_A} \arctan \left[\frac{C_1 + 2R}{\sqrt{-C_1^2 + 4C_2}} \right] \right) dU d\tilde{v}. \quad (\text{C10})$$

There is no singularity other than $R = 0$ (that corresponds to the central point $r = 0$) in this metric.

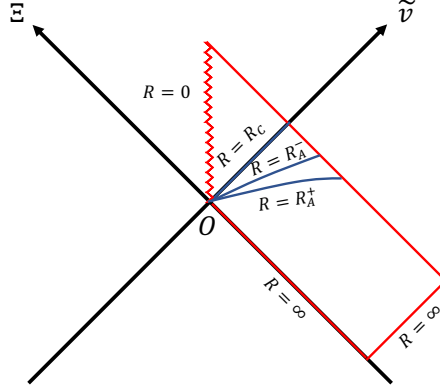


Fig. C1 Penrose diagram of the collapse domain in the case of $b = 0$.

Below, we consider properties of R -constant surfaces. For this purpose, we compute the normal of the R -constant surfaces, $n_\mu = \nabla_\mu R$. From Eq. (C2), the $(u, \tilde{v}, \theta, \phi)$ -components of n_μ are

$$n_\mu = \frac{f\alpha - 2R}{2} (-1, \tilde{v}, 0, 0), \quad (\text{C11})$$

and the norm of this vector is computed as

$$n_\mu n^\mu = \frac{f\alpha - 2R}{M_0^2 \alpha \tilde{v}^2}. \quad (\text{C12})$$

From this, R -constant surfaces with $R < R_C$, $R = R_C$, and $R > R_C$ are timelike, null, and spacelike since $n_\mu n^\mu > 0$, $n_\mu n^\mu = 0$, and $n_\mu n^\mu < 0$ hold, respectively.

Let us consider the location of several R -constant surfaces. First, we consider the homothetic Killing horizon at $R = R_C$. Substituting $R = R_C$ into Eq. (C9), we find $U = 0$. Second, we consider $R = \infty$. Taking the limit $R \rightarrow \infty$ in Eq. (C9), we have $U/\tilde{v}^{\kappa_C} = -\infty$. This means $U = -\infty$ or $\tilde{v} = 0$. Third, the central singularity $R = 0$ is located at

$$\frac{U}{\tilde{v}^{\kappa_C}} = R_C (C_2)^{\frac{\kappa_C}{\kappa_B}} \exp \left(\frac{\kappa_C}{\kappa_A} \arctan \left[\frac{C_1}{\sqrt{-C_1^2 + 4C_2}} \right] \right). \quad (\text{C13})$$

This is a timelike surface in the domain $U > 0$ and $\tilde{v} > 0$. Finally, let us consider the location of the boundary of the trapped region, or the (inner and outer) apparent horizons. As shown in Appendix B, apparent horizons satisfy $f(R) = 0$. This is equivalent to $y(R) = 0$, and there are two solutions R_A^+ and R_A^- (here we suppose $R_A^- < R_A^+$). From Fig. 2, both R_A^+ and R_A^- are larger than R_C , and therefore, the apparent horizons are spacelike hypersurfaces. We also remark that R can take arbitrary positive values at the point $(U, \tilde{v}) = (0, 0)$. Therefore, all R -constant surfaces plunge into this point.

We now present the Penrose diagram of the collapse domain, $-v_i \leq v \leq 0$. The coordinate range of \tilde{v} is finite, $0 \leq \tilde{v} \leq 1$, while that of U is infinite. In order to present the U direction in a finite domain, we introduce the compactified coordinate by $U = \tan \Xi$ with $-\pi/2 < \Xi < \pi/2$. In the coordinates (Ξ, \tilde{v}) , the past null infinity \mathcal{I}^- is located at $\Xi = -\pi/2$, and the homothetic Killing horizon is located at $\Xi = 0$. The central singularity $R = 0$ is a timelike surface in the domain $\Xi > 0$ and $\tilde{v} > 0$, and the apparent horizons at $R = R_A^\pm$ are spacelike

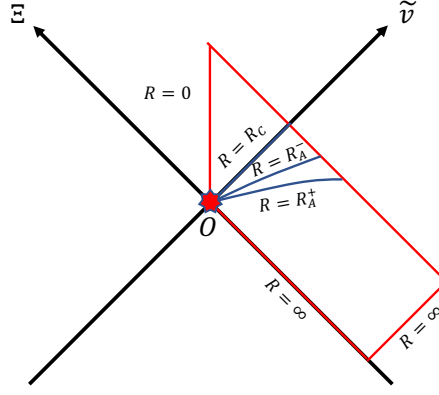


Fig. C2 Penrose diagram of collapse domain in the case of $b \neq 0$.

surfaces in the domain $\Xi < 0$ and $\tilde{v} > 0$. From these observations, we obtain the diagram of Fig. C1.

C.2. The case of time-dependent regularization

We now briefly comment on the case that Eq. (60) with $b \neq 0$ is used for the function $F_-(v, r)$. In this case, the function $y(R)$ of Eq. (C3) is modified as

$$y(R) = \frac{R^4 - 2R^3 + q^2R^2 + (2R + q^2)b^2}{2R[R^4 + (2R + q^2)b^2]}. \quad (\text{C14})$$

The primary difference from Eq. (C3) is that the divergence at $R \rightarrow 0$ becomes weaker. Equation (C3) behaves as $y(R) \approx q^2/2R^3$ while Eq. (C14) behaves as $y(R) \approx 1/2R$ at $R \ll 1$. Except that, the behavior of $y(R)$ of Eq. (C14) is similar to that of $y(R)$ of Eq. (C3) as long as b is sufficiently small, and the similar discussion holds also for the case $b \neq 0$. Namely, $y(R)$ takes extremal values at $R = R_{\pm}$, and Eq. (C14) has one, two, and three positive solutions in the case that $1/\alpha > y(R_+)$, $1/\alpha = y(R_+)$, and $1/\alpha < y(R_+)$, respectively.

We consider the case that there is only one solution to Eq. (C14) (denoted as $R = R_C$). Although carrying out the integral of Eq. (C2) analytically seems to be difficult, we can proceed a formal discussion as follows. We can write $f\alpha - 2R$ as

$$f\alpha - 2R = -2(R - R_C)\kappa(R) \quad (\text{C15})$$

with some positive definite function $\kappa(R)$ with the property $\kappa(0) = \alpha/2R_C$ and $\kappa(\infty) = 1$. Equation (C2) is rewritten as

$$u = \ln \tilde{v} + \frac{1}{\kappa_C} \ln |R - R_C| + G(R) \quad (\text{C16})$$

with $\kappa_C := \kappa(R_C)$ and

$$G(R) = \int \frac{1/\kappa(R) - 1/\kappa_C}{R - R_C} dR. \quad (\text{C17})$$

Note that the integrand of $G(R)$ is regular both at $R = 0$ and $R = R_C$. Introducing the coordinate U in the same manner as Eq. (C8), we have

$$\frac{U}{\tilde{v}^{\kappa_C}} = -(R - R_C) \exp[\kappa_C G(R)]. \quad (\text{C18})$$

In the (U, \tilde{v}) -coordinates, the metric is written as

$$ds^2 = -\frac{2\alpha M_0^2}{\kappa_C} \tilde{v}^{1-\kappa_C} \kappa(R) \exp[-\kappa_C G(R)] dU d\tilde{v}. \quad (\text{C19})$$

In the case $b \neq 0$, the metric is regular on the worldline of the central point, $R = 0$, except at $(U, \tilde{v}) = (0, 0)$. The point $(U, \tilde{v}) = (0, 0)$ is a curvature singularity by the fact that all R -constant surfaces plunges into this point. The Penrose diagram can be drawn in the similar manner to the $b = 0$ case. The only difference is that $R = 0$ becomes the regular center except at $(U, \tilde{v}) = (0, 0)$, and the diagram of Fig. C2 is obtained.

D. Geometrical quantities of ingoing Vaidya spacetimes and the characteristic of apparent horizons

In this appendix, we summarize the calculation of geometric quantities of the (partly) regularized charged Vaidya spacetimes. In Appendix D.1, we present the formula for the curvature invariants constructed from the Riemann tensor. In Appendix D.2, we examine the behavior of the Einstein tensor in the ingoing Vaidya spacetimes in detail, and whether the null and dominant energy conditions (NEC and DEC) are satisfied in the framework of general relativity. We examine the validity of the characteristic of the apparent horizons in Appendix D.3.⁵

D.1. Curvature invariants

For the metric of Eq. (1), the representative geometric invariants that are constructed from the Riemann tensor $\mathcal{R}_{\mu\nu\rho\sigma}$ are calculated as

$$\mathcal{R} = -\frac{2(F_- - 1)}{r^2} - \frac{4F_{-,r}}{r} - F_{-,rr}, \quad (\text{D1a})$$

$$\mathcal{R}_{\mu\nu}\mathcal{R}^{\mu\nu} = 2\left(\frac{F_- - 1}{r^2} + \frac{F_{-,r}}{r}\right)^2 + 2\left(\frac{F_{-,r}}{r} + \frac{F_{-,rr}}{2}\right)^2, \quad (\text{D1b})$$

$$\mathcal{R}_{\mu\nu\rho\sigma}\mathcal{R}^{\mu\nu\rho\sigma} = 4\left(\frac{F_- - 1}{r^2}\right)^2 + 4\left(\frac{F_{-,r}}{r}\right)^2 + F_{-,rr}. \quad (\text{D1c})$$

D.1.1. Time-dependent regularization. In the self-similar case studied in Sect. 4, $F_-(v, r)$ is expressed as a function $f(R)$ with $R = r/M(v)$ as Eq. (61). In this case, the geometric invariants are

$$\mathcal{R} = -\frac{1}{M(v)^2} \left[\frac{2(f(R) - 1)}{R^2} + \frac{4f'(R)}{R} + f''(R) \right], \quad (\text{D2a})$$

$$\mathcal{R}_{\mu\nu}\mathcal{R}^{\mu\nu} = \frac{2}{M(v)^4} \left[\left(\frac{f(R) - 1}{R^2} + \frac{f'(R)}{R} \right)^2 + \left(\frac{f'(R)}{R} + \frac{f''(R)}{2} \right)^2 \right], \quad (\text{D2b})$$

$$\mathcal{R}_{\mu\nu\rho\sigma}\mathcal{R}^{\mu\nu\rho\sigma} = \frac{1}{M(v)^4} \left[4\left(\frac{f(R) - 1}{R^2}\right)^2 + 4\left(\frac{f'(R)}{R}\right)^2 + (f''(R))^2 \right]. \quad (\text{D2c})$$

⁵ Appendixes D.2 and D.3 have been added by a strong suggestion by the referee, and many of the analyses were helped and inspired by referee's report.

These geometric invariants diverge in the limit $M(v) \rightarrow 0$ for a fixed R , indicating the presence of the spacetime singularity. In particular, $f(R)$ behaves as $f(R) \approx 1 + R^2/b^2$ in the neighborhood of $R = 0$, and this gives Eqs. (67a)–(67c) in the main text.

D.1.2. Constant regularization. In the constant regularization in Sect. 5, the function $F_-(v, r)$ behaves as $F_-(v, r) \approx 1 + r^2/\ell^2$ in the neighborhood of $r = 0$. Then, the geometric invariants take the values

$$\mathcal{R}|_{r=0} = -12/\ell^2, \quad (\text{D3a})$$

$$\mathcal{R}_{\mu\nu}\mathcal{R}^{\mu\nu}|_{r=0} = 36/\ell^4, \quad (\text{D3b})$$

$$\mathcal{R}_{\mu\nu\rho\sigma}\mathcal{R}^{\mu\nu\rho\sigma}|_{r=0} = 24/\ell^4, \quad (\text{D3c})$$

at $r = 0$.

D.2. Einstein tensor

Although we consider that the regularization of the Vaidya spacetime would be realized by modification of the gravity theory, it is interesting to discuss what kind of matter is required in order to realize the regularized Vaidya spacetime within the framework of general relativity. For this reason, we examine the properties of the Einstein tensor in detail. For the metric given by Eq. (1), the nonzero components of the Einstein tensor $G^\mu{}_\nu$ are

$$G^v{}_v = G^r{}_r = \frac{F_- - 1}{r^2} + \frac{F_{-,r}}{r}, \quad (\text{D4a})$$

$$G^\theta{}_\theta = G^\phi{}_\phi = \frac{F_{-,r}}{r} + \frac{F_{-,rr}}{2}, \quad (\text{D4b})$$

$$G^r{}_v = -\frac{F_{-,v}}{r}. \quad (\text{D4c})$$

Adopting the same tetrad $(e^a)_\mu$ as Eqs. (52a)–(52d) but F being replaced by F_- , the tetrad components of the Einstein tensor is written as

$$G^{ab} = \begin{pmatrix} \rho & 0 & 0 & 0 \\ 0 & -\rho & 0 & 0 \\ 0 & 0 & p & 0 \\ 0 & 0 & 0 & p \end{pmatrix} + \begin{pmatrix} \nu & \nu & 0 & 0 \\ \nu & \nu & 0 & 0 \\ 0 & 0 & 0 & 0 \\ 0 & 0 & 0 & 0 \end{pmatrix}, \quad (\text{D5})$$

(which belongs to the canonical form of type II [37], see also [38]), where

$$\rho = \frac{1 - F_- - rF_{-,r}}{r^2}, \quad (\text{D6a})$$

$$p = \frac{F_{-,r}}{r} + \frac{F_{-,rr}}{2}, \quad (\text{D6b})$$

$$\nu = -\frac{F_{-,v}}{r}. \quad (\text{D6c})$$

In the case of the charged ingoing Vaidya spacetime, the first and second terms of the right-hand side of Eq. (D5) correspond to the electromagnetic part and the matter part of Eq. (4), respectively (except for the factor 8π), and the null vector k^μ of Eq. (8) is expressed as $k^\mu = (e^0)^\mu - (e^1)^\mu$ in terms of the tetrad basis here. ρ , p , and ν here are related to the quantities in Eqs. (6) and (9) as $\rho/8\pi = \tilde{\rho} = -\tilde{p}_r$, $p/8\pi = \tilde{p}_\theta = \tilde{p}_\phi$, and $\nu/8\pi = \tilde{\nu}$.

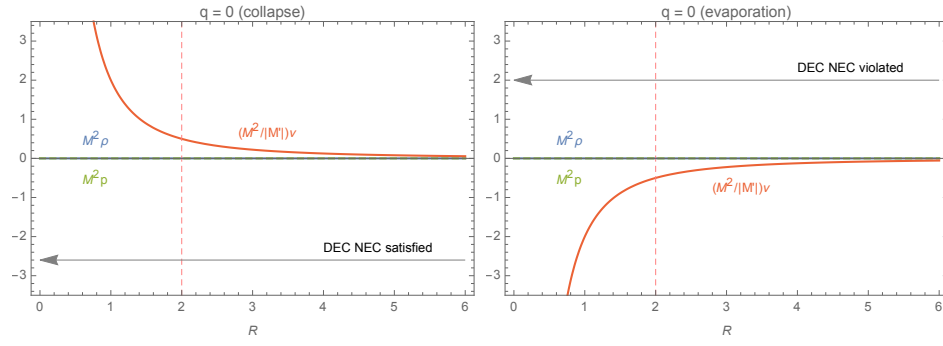


Fig. D1 The behavior of $M^2\rho$, M^2p , and $(M^2/M')\nu$ as functions of R in the case of an uncharged ingoing Vaidya spacetime in the collapsing phase (left panel) and in the evaporation phase (right panel). The vertical red dashed line indicates the location of the apparent horizon.

In terms of the quantities ρ , p , and ν , the NEC is equivalent to

$$\nu \geq 0 \quad \text{and} \quad \rho + p \geq 0, \quad (\text{D7})$$

while the DEC is equivalent to

$$\nu \geq 0 \quad \text{and} \quad \rho \geq |p|. \quad (\text{D8})$$

Below, we examine the behavior of ρ , p , and ν , and whether the NEC and DEC are satisfied.

D.2.1. Self-similar case. In the self-similar case, the function F_- has the form $F_- = f(R)$ with $R = r/M(v)$. In this case, the three quantities have the form

$$\rho = \frac{1}{M(v)^2} \frac{1 - f - Rf'(R)}{R^2}, \quad (\text{D9a})$$

$$p = \frac{1}{M(v)^2} \left(\frac{f'(R)}{R} + \frac{f''(R)}{2} \right), \quad (\text{D9b})$$

$$\nu = \frac{M'(v)}{M(v)^2} f'(R). \quad (\text{D9c})$$

In the (uncharged) ingoing Vaidya spacetime with $q = 0$, where $f(R)$ is given by Eq. (17), we have $\rho = p = 0$ and

$$\nu = \frac{M'}{M^2} \frac{2}{R^2}. \quad (\text{D10})$$

Figure D1 shows the behavior of $M^2\rho$, M^2p , and $(M^2/M')\nu$ as functions of R in the collapsing phase (left panel) and in the evaporation phase (right panel). In the collapsing phase where $M'(v)$ is positive, ν is positive for an arbitrary R , and thus, both the NEC and DEC are satisfied everywhere. On the other hand, in the evaporating phase where $M'(v)$ is negative, ν becomes negative and the NEC and DEC are violated for arbitrary R . This is because negative energy flows into the central region.

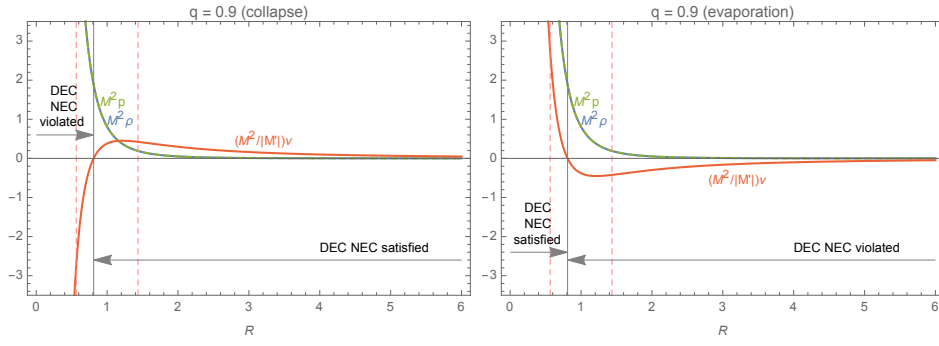


Fig. D2 The same as Fig. D1 but for $q = 0.90$. The left and right vertical red dashed lines indicate the locations of the inner and outer apparent horizons, respectively.

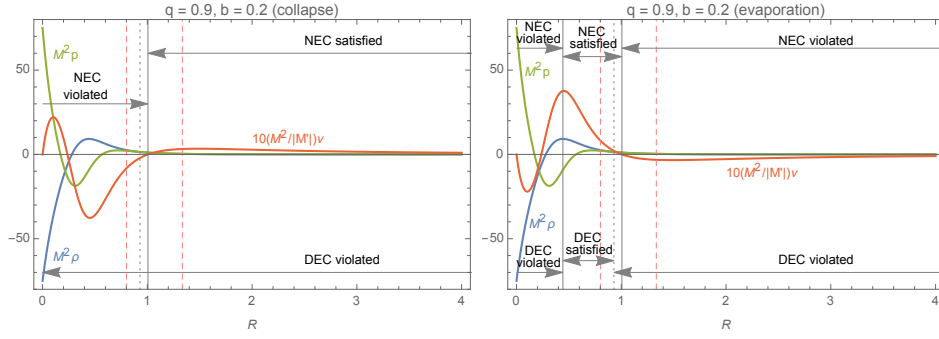


Fig. D3 The same as Fig. D2 but for a partly regularized spacetime with $q = 0.90$ and $b = 0.20$. As for the function ν , we plot $10(M^2/|M'|)\nu$ for visibility.

In the case of charged ingoing Vaidya spacetime with $q \neq 0$ given by Eq. (17), p , ρ , and ν are calculated as

$$p = \rho = \frac{q^2}{M^2 R^4}, \quad (\text{D11a})$$

$$\nu = \frac{2M'}{M^2 R^3} (R - q^2). \quad (\text{D11b})$$

ρ and p have the positive values, and this corresponds to the energy density and pressures of the electric field. Figure D1 shows the case of $q = 0.9$. In the collapsing phase, ν is positive for $R > q^2$ while it becomes negative for $R < q^2$ (as Ori pointed out in [30]). Correspondingly, around the center, the NEC and DEC are violated. Hence, the NEC and DEC are violated and satisfied for $R < q^2$ and $R > q^2$, respectively. In the evaporating phase, the opposite happens: negative energy flows to the center for large R , but it becomes positive around the center. Hence, the NEC and DEC are satisfied and violated for $R < q^2$ and $R > q^2$, respectively.

We now turn to the partly regularized spacetime with $b \neq 0$ given by Eq. (61). p , ρ , and ν are given as

$$\rho = \frac{q^2 R^4 + b^2(12R^2 + 4q^2 R - 3q^4)}{M^2[R^4 + b^2(2R + q^2)]^2}, \quad (\text{D12a})$$

$$p = \frac{q^2 R^8 + 6b^2 R^4(4R^2 + q^2 R - 2q^4) + b^4(-24R^3 - 28q^2 R^2 - 6q^4 R + 3q^6)}{M^2[R^4 + b^2(2R + q^2)]^3}, \quad (\text{D12b})$$

$$\nu = \frac{M' 2R [R^5 - q^2 R^4 + b^2(-4R^2 - 2q^2 R + q^4)]}{M^2 [R^4 + b^2(2R + q^2)]^2}. \quad (\text{D12c})$$

The behavior of ρ , p , and ν are relatively complicated as shown in Figure D3. The value of ρ is positive for large R , and becomes negative as R is decreased. It takes the value $\rho = -3/b^2 M^2$ at $r = 0$. The value of p is positive for large R . As R is decreased, it once becomes negative, and then, becomes positive again, and takes the value $p = 3/b^2 M^2$ at $r = 0$. In the collapsing phase, the value of ν is positive for large R . As R is decreased, it once becomes negative, and then, becomes positive again, and takes the value $\nu = 0$ at $r = 0$. The DEC is violated everywhere. The NEC is satisfied in the distant region, while it is violated around the center. In the evaporating phase, the behavior of ν is opposite. There are two regions where both the NEC and DEC are violated around the center and at the distant region. Between them, there is a region where the NEC and DEC are satisfied. There is also a small region where the NEC is satisfied but the DEC is violated.

D.2.2. Completely regularized case. In the completely regularized case, we have

$$\rho = \frac{M^2 [q^2 r^4 + \ell^2(12r^2 + 4q^2 M r - 3q^4 M^2)]}{[r^4 + \ell^2(2M r + q^2 M^2)]^2}, \quad (\text{D13a})$$

$$p = \frac{M^2 [q^2 r^8 + 6\ell^2 r^4(4r^2 + q^2 M r - 2q^4 M^2)]}{[r^4 + \ell^2(2M r + q^2 M^2)]^3} + \frac{\ell^4 M^3 [-24r^3 - 28q^2 M r^2 + 3q^4 M^2(-2r + q^2 M)]}{[r^4 + \ell^2(2M r + q^2 M^2)]^3}, \quad (\text{D13b})$$

$$\nu = \frac{2r^2 M' (r^4 - q^2 M r^3 - 2\ell^2 q^2 M^2)}{[r^4 + \ell^2(2M r + q^2 M^2)]^2}, \quad (\text{D13c})$$

from Eq. (58). Here, we consider the case of $q = 0.9$ with the linear mass function considered in the right panel of Fig. 11. The collapsing phase is $-v_i \leq v \leq 0$ and the evaporation phase is $0 \leq v \leq v_f$, where $v_i = 6\ell$ and $v_f = 60\ell$.

Figure D4 shows the snapshots of ρ (top left), p (top right), and ν (bottom) as functions of r for $v = -5, -4, -3, -2, -1, 0, 10, 20, 30, 40, 50$ in the unit $\ell = 1$. The value of ρ is positive for large r , becomes negative as r is decreased, and has the value $\rho = -3/\ell^2$ at $r = 0$. The value of p is positive for large r , once becomes negative as r is decreased, and then, becomes positive again, and has the value $p = 3/\ell^2$ at $r = 0$. The functions $\rho(r)$ and $p(r)$ for some $v > 0$ in the evaporation phase are the same as those at time $-(v_i/v_f)v$ in the collapsing phase, because these functions are determined by the value of M . In the collapsing phase, the value of ν is positive for large r and negative for small r . The function $\nu(r)$ for some $v > 0$ in the evaporation phase is the same as that at $-(v_i/v_f)v$ except that it is flipped about the horizontal axis (i.e., the sign is changed) and the absolute value is decreased by the factor of v_i/v_f .

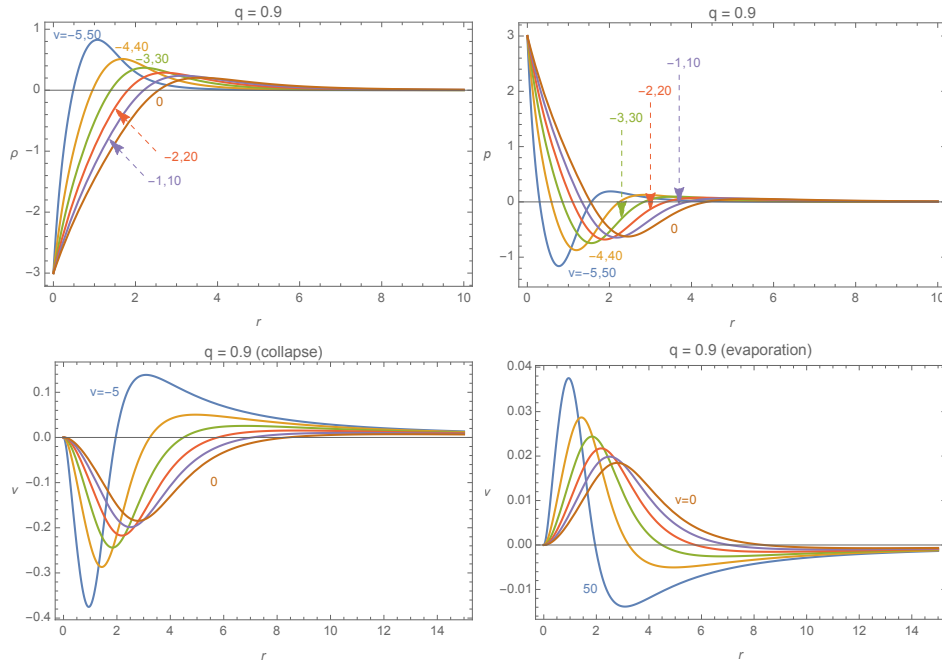


Fig. D4 The snapshots of ρ (top left), p (top right), and ν (bottom left and bottom right) as functions of r for $v = -5, -4, -3, -2, -1, 0, 10, 20, 30, 40$, and 50 in the unit $\ell = 1$.

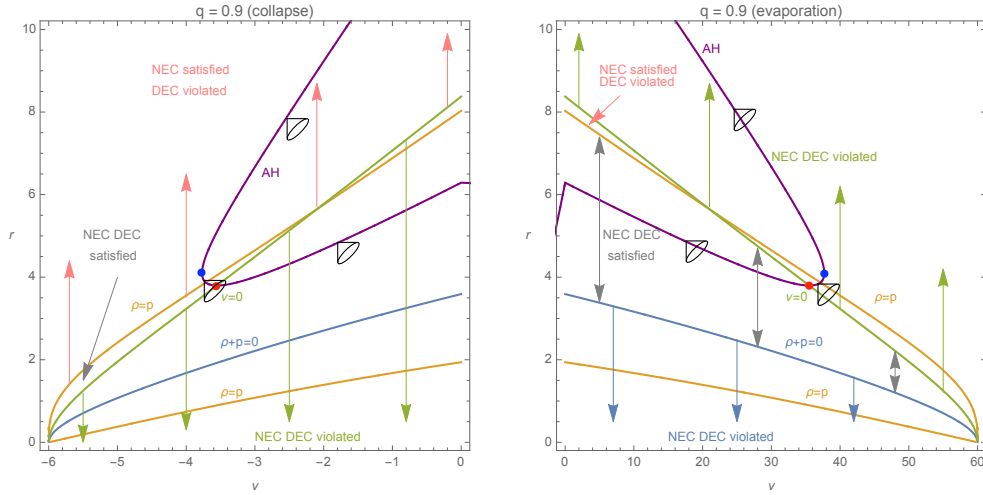


Fig. D5 The domains where the NEC and DEC are satisfied/violated in the (v, r) -plane in the collapsing phase (left panel) and in the evaporation phase (right panel). The purple curve is the location of the apparent horizons. At blue and red points, the apparent horizon changes its characteristic. The light cones at some points on the apparent horizon are also indicated.

Figure D5 shows the domains where the NEC and DEC are satisfied/violated in the (v, r) -plane in the collapsing phase (left panel) and in the evaporation phase (right panel). In the collapsing phase, the NEC is violated around the center (as indicated by green arrows) and is satisfied at the distant region (as indicated by red arrows). The DEC is violated in

almost all regions, except the narrow region indicated by the grey arrow. In the evaporation phase, the NEC and DEC are violated around the center (as indicated by blue arrows) and at the distant region (as indicated by green arrows). Between them, there is a region where the NEC and DEC are satisfied as indicated by grey arrows. There is also a narrow region (indicated by the red arrow) where the NEC is satisfied but the DEC is violated.

D.3. Characteristic of apparent horizons

We discuss the condition that determines the characteristic of the sequence of the apparent horizon (i.e., whether it is spacelike, null, timelike), and provide a support for the validity of our Penrose diagrams in the main text.

D.3.1. General criteria. The criteria for determining the characteristics of the apparent horizons can be derived as follows. Since $F_- = 0$ holds on the apparent horizon, we have

$$F_{-,v}dv + F_{-,r}dr = 0 \quad (\text{D14})$$

on the sequence of the apparent horizons. Substituting this relation into the metric together with $F_- = 0$, we have the induced metric on the apparent horizon,

$$ds^2 = -\frac{2F_{-,v}}{F_{-,r}}dv^2 + r^2d\Omega^2. \quad (\text{D15})$$

In the case of self-similar spacetimes, the function F_- is given by $F_-(v, r) = f(R)$ with $R = r/M(v)$. Substituting $F_{-,v} = -(M'/M)Rf'(R)$ and $F_{-,r} = f'(R)/M$ into Eq. (D15), we have

$$ds^2 = 2M'Rdv^2 + r^2d\Omega^2, \quad (\text{D16})$$

that is, the apparent horizon is spacelike if $M' > 0$ and is timelike if $M' < 0$. This means that the apparent horizon is spacelike in the collapsing phase, and is timelike in the evaporation phase. This result is consistent with our Penrose diagrams for the self-similar spacetimes.

In the case that the spacetime is not self-similar, we have to use Eq. (D15). Let us recall the fact that ν is given by Eq. (D6c), and hence, the metric on the apparent horizons is rewritten as

$$ds^2 = \frac{2r\nu}{F_{-,r}}dv^2 + r^2d\Omega^2. \quad (\text{D17})$$

We now consider the case where $F_- = 1$ holds at infinity $r = \infty$ and at the center $r = 0$, and the inner and outer apparent horizons exist. In such a situation, $F_{-,r} < 0$ holds on the inner apparent horizon, while $F_{-,r} > 0$ holds on the outer apparent horizon. This discussion gives the following criteria:

- The outer apparent horizon is spacelike if $\nu > 0$ and is timelike if $\nu < 0$;
- The inner apparent horizon is timelike if $\nu > 0$ and is spacelike if $\nu < 0$.

There are two possibilities where the sequence of the apparent horizons becomes null: The case $F_{-,r} = 0$ and the case $\nu = 0$. In the former case, the sequence of the apparent horizons becomes tangential to a $v = \text{constant}$ surface, and it is the point where the inner and outer apparent horizons are connected. In the latter case, the sequence of the apparent horizons becomes tangential to a $u = \text{constant}$ surface, and it occurs at the point where the apparent horizon changes its characteristic in each of the outer and inner sequences. Let us examine whether Fig. D5 is consistent with these criteria. The outer apparent horizon is spacelike

(timelike) for $v < 0$ ($v > 0$) and it is located in the region $\nu > 0$ ($\nu < 0$). In the region around $v = 0$ (i.e., between the blue and red points in each panel), the inner apparent horizon is spacelike (timelike) for $v < 0$ ($v > 0$) and it is located in the region $\nu < 0$ ($\nu > 0$). At some values of v (i.e., at red points), the inner apparent horizon crosses the contour surface of $\nu = 0$, and change of the characteristic occurs there (i.e., dr/dv of the apparent horizon becomes zero). Therefore, our results satisfy the above criteria, indicating the validity of our results.

D.3.2. Consistency with Hayward's theorem. Here, we briefly comment on the consistency of our results on the apparent horizons with Hayward's theorem [36]. In the framework of general relativity, Hayward has proven the fact that if the NEC holds, an outer apparent horizon is spacelike, and an inner apparent horizon is timelike.

In the unregularized charged ingoing Vaidya spacetime where $f(R)$ is given by Eq. (17), ρ and p are both positive, and hence, $\rho + p$ is also always positive. Therefore, whether the NEC is satisfied or not is solely determined by the sign of ν . From Eq. (31), the location of the apparent horizons, R_A^\pm , are written as

$$R_A^\pm = \frac{q^2}{1 \mp \sqrt{1 - q^2}}, \quad (\text{D18})$$

which indicates $R_A^+ > q^2$ and $R_A^- < q^2$. Since Eq. (D11b) tells that ν is positive and negative in the regions $R > q^2$ and $R < q^2$, respectively, ν is positive (negative) at $R = R_A^+$ in the collapsing (evaporating) phase, and ν is negative (positive) at $R = R_A^-$ in the collapsing (evaporating) phase. Therefore, Hayward's theorem states that the outer (inner) apparent horizon must be spacelike (timelike) in the collapsing (evaporating) phase. On the characteristic of the outer (inner) apparent horizon in the evaporating (collapsing) phase, Hayward's theorem tells nothing. These are consistent with Fig. 5.

In the partly regularized model where $f(R)$ is given by Eq. (61), it is difficult to discuss whether the null energy condition is satisfied based on the exact formulas for the location of the apparent horizon, $R = R_A^\pm$, because $f(R)$ is complicated. However, as long as the value of b^2 is small, the values of R_A^\pm are shifted by $O(b^2)$ from the $b = 0$ case. Thus, the values of $\rho + p$ and ν at $R = R_A^\pm$ are also different from the $b = 0$ case by $O(b^2)$. Therefore, the same conclusion as the $b = 0$ case must hold, and Fig. 10 is consistent with Hayward's theorem.

Finally, we discuss the completely regularized case using Fig. D5 as an example. Although one of the null energy conditions, $\rho + p \geq 0$, is violated around the center, this condition is satisfied on the apparent horizons. Therefore, whether the NEC is satisfied or not is solely determined by the sign of ν . Then, from the criteria for the characteristic of the apparent horizons in terms of ν obtained in Appendix D.3.1, we conclude that the characteristics of the apparent horizons are consistent with Hayward's theorem.

E. Connecting the ingoing and outgoing charged Vaidya spacetimes

In Sects. 2, 4 and 5, we studied the structure of the ingoing charged Vaidya spacetimes. In order to make a model for the evaporation of a black hole, we must cut and glue the ingoing and outgoing Vaidya spacetimes on some timelike hypersurface (e.g., the procedure to make the right panel from the left panel in Fig. 5). We discuss the method of this procedure here. The metrics of ingoing and outgoing Vaidya spacetimes are given by Eqs. (1)

and (12), respectively. The two spacetimes are connected on a timelike hypersurface, Γ . The surface Γ is specified by $v = v_-(r)$ and $u = u_+(r)$ in the ingoing and outgoing Vaidya spacetimes, respectively. For the connection to be continuous, the two induced metrics on the hypersurface Γ must coincide,

$$F_-(v_-(r), r)(v'_-)^2 - 2v'_- = F_+(u_+(r), r)(u'_+)^2 + 2u'_+. \quad (\text{E1})$$

E.1. Self-similar case

Here we consider the self-similar spacetimes studied in Sects. 2 and 4. As for the ingoing Vaidya spacetime, the function $F_-(v, r)$ is chosen to be the same as Eq. (58), but here, we add the subscript “−” to $M(v)$ and $Q(v)$ as $M_-(v)$ and $Q_-(v)$, respectively. The function $F_-(v, r)$ is

$$F_-(v, r) = 1 - \frac{(2M_-(v)r - Q_-(v)^2)r^2}{r^4 + (2M_-(v)r + Q_-(v)^2)M_-(v)^2b^2}, \quad (\text{E2})$$

with $Q_-(v) = qM_-(v)$. The mass function is the same as Eq. (14), and we focus on the range $0 \leq v \leq v_f$,

$$M_-(v) = M_0 \left(1 - \frac{v}{v_f}\right). \quad (\text{E3})$$

In the same manner to Secs 2 and 4, the coordinate R is introduced by $R = r/M_-(v)$, and the surface Γ on which the outgoing Vaidya spacetime is glued is supposed to be $R = R_H$. Then, the function $v_-(r)$ becomes

$$v_-(r) = v_f \left(1 - \frac{r}{M_0 R_H}\right). \quad (\text{E4})$$

The derivative of $v_-(r)$ is constant, $v'_- = -v_f/M_0 R_H$. The function $F_-(v, r)$ is expressed only in terms of R , and it is denoted as $f(R)$ like Eq. (61). Note that on the surface Γ , the relations $F_-(v_-(r), r) = f(R_H)$ and $M_-(v_-(r)) = r/R_H$ hold.

E.1.1. Procedure for connecting two spacetimes. For the function $F_+(u, r)$ in the outer domain, we assume the same formula as $F_-(v, r)$ but $M_-(v)$ and $Q_-(v)$ being replaced by $M_+(u)$ and $Q_+(u)$, respectively:

$$F_+(u, r) = 1 - \frac{(2M_+(u)r - Q_+(u)^2)r^2}{r^4 + (2M_+(u)r + Q_+(u)^2)M_+(u)^2b^2}, \quad (\text{E5})$$

with $Q_+(u) = qM_+(u)$. We would like to determine the two functions $u_+(r)$ and $M_+(u)$. Since there is only one condition given by Eq. (E1) for these functions, we have to impose one more condition. Here, we assume the continuity of the two mass functions on Γ , $M_-(v_-(r)) = M_+(u_+(r))$, as a natural condition.⁶ This means that $F_-(v_-(r), r) = F_+(u_+(r), r) = f(R_H)$ holds on Γ . Using this condition, Eq. (E1) is solved as

$$u'_+ = v'_- - \frac{2}{f(R_H)}, \quad (\text{E6})$$

where we chose the solution that satisfies $u'_+ < 0$. Integrating this equation, $u_+(r) = u'_+(r - M_0 R_H)$ is obtained. The advanced time $u_f := u_+(0)$ at which the charged star completely

⁶ In Ref. [10], the condition $v_-(r) = u_+(r)$ is used and this condition leads to a different model. The degree of freedom for choosing such conditions corresponds to what kind of discontinuity in the extrinsic curvature appears on Γ .

evaporates is given as

$$u_f = v_f + \frac{2M_0 R_H}{f(R_H)}. \quad (\text{E7})$$

Using u_f , the function $u_+(r)$ is expressed as

$$u_+(r) = u_f \left(1 - \frac{r}{M_0 R_H} \right), \quad (\text{E8})$$

and the mass function $M_+(u)$ that realizes the condition $M_-(v_-(r)) = M_+(u_+(r)) = r/R_H$ is

$$M_+(u) = M_0 \left(1 - \frac{u}{u_f} \right). \quad (\text{E9})$$

E.1.2. The surface stress tensor. The surface Γ is a singular hypersurface in the sense of Israel's definition [47]. To see this, we calculate the extrinsic curvature of Γ for both ingoing and outgoing Vaidya spacetime. Recall that the surface Γ is given by $R = R_H$ in the ingoing Vaidya spacetime. In the outgoing Vaidya spacetime, Γ is also given by $R = R_H$ introducing the coordinate R by $R = r/M_+(u)$, since $M_-(v) = M_+(u)$ holds on Γ . To simplify the presentation, we calculate the extrinsic curvature in a unified manner by introducing $z_- = v$ and $z_+ = u$. The two metrics are

$$ds^2 = -F_{\pm}(z_{\pm}, r) dz_{\pm}^2 \mp 2dz_{\pm} dr + r^2 d\Omega^2. \quad (\text{E10})$$

Introducing $R = r/M_{\pm}(z_{\pm})$, the metric components in the $(z_{\pm}, R, \theta, \phi)$ coordinates are expressed as

$$g_{\mu\nu} = \begin{pmatrix} -(f(R) \pm 2M'_{\pm} R) & \mp M_{\pm}(z_{\pm}) & 0 & 0 \\ \mp M_{\pm}(z_{\pm}) & 0 & 0 & 0 \\ 0 & 0 & R^2 M_{\pm}(z_{\pm})^2 & 0 \\ 0 & 0 & 0 & R^2 M_{\pm}(z_{\pm})^2 \sin^2 \theta \end{pmatrix}. \quad (\text{E11})$$

The inverse metrics are

$$g^{\mu\nu} = \frac{1}{M_{\pm}(z_{\pm})^2} \begin{pmatrix} 0 & \mp M_{\pm}(z_{\pm}) & 0 & 0 \\ \mp M_{\pm}(z_{\pm}) & f(R) \pm 2M'_{\pm} R & 0 & 0 \\ 0 & 0 & R^{-2} & 0 \\ 0 & 0 & 0 & R^{-2} \sin^{-2} \theta \end{pmatrix}, \quad (\text{E12})$$

and the unit normal to the hypersurface $R = \text{constant}$ is given by

$$n_{\mu}^{\pm} = \frac{M_{\pm}}{\sqrt{f(R) \pm 2M'_{\pm} R}} (0, 1, 0, 0). \quad (\text{E13})$$

The unit timelike tangent vector to Γ is calculated as

$$\hat{t}^{\mu} = \frac{1}{\sqrt{f(R) \pm 2M'_{\pm} R}} (1, 0, 0, 0). \quad (\text{E14})$$

The two spacelike unit tangent vectors are given as

$$\hat{\theta}^{\mu} = \frac{1}{RM_{\pm}(z_{\pm})} (0, 0, 1, 0), \quad (\text{E15a})$$

$$\hat{\phi}^{\mu} = \frac{1}{RM_{\pm}(z_{\pm}) \sin \theta} (0, 0, 0, 1). \quad (\text{E15b})$$

The vectors \hat{t}^{μ} , $\hat{\theta}^{\mu}$, and $\hat{\phi}^{\mu}$ consist of the triad basis of the hypersurface Γ .

The extrinsic curvatures K_{ij}^\pm are calculated below, where i, j denotes the components with respect to the triad basis, \hat{t}^μ , $\hat{\theta}^\mu$, and $\hat{\phi}^\mu$. Due to the spherical symmetry, the only nonzero components are $K_{\hat{t}\hat{t}}^\pm$, $K_{\hat{\theta}\hat{\theta}}^\pm$, and $K_{\hat{\phi}\hat{\phi}}^\pm$, where $K_{\hat{t}\hat{t}}^\pm = \hat{t}^\mu \hat{t}^\nu \nabla_\mu n_\nu^\pm$ and so on. A calculation gives

$$K_{\hat{t}\hat{t}}^\pm = -\frac{f'(R)}{2M_\pm(z_\pm)\sqrt{f(R) \pm 2M'_\pm R}}, \quad (\text{E16a})$$

$$K_{\hat{\theta}\hat{\theta}}^\pm = K_{\hat{\phi}\hat{\phi}}^\pm = \frac{f(R) - M'_\pm R}{RM_\pm(z_\pm)\sqrt{f(R) \pm 2M'_\pm R}}. \quad (\text{E16b})$$

Evaluating these values on $R = R_H$ and substituting $M'_- = -M_0/v_f$, $M'_+ = -M_0/u_f$, and Eq. (E7), we have

$$K_{\hat{t}\hat{t}}^+ = -\frac{f'(R_H)}{2f(R_H)M_+(u)}\sqrt{\frac{v_f f(R_H) + 2M_0 R_H}{v_f}}, \quad (\text{E17a})$$

$$K_{\hat{t}\hat{t}}^- = -\frac{f'(R_H)}{2M_-(v)}\sqrt{\frac{v_f}{v_f f(R_H) + 2M_0 R_H}}, \quad (\text{E17b})$$

$$K_{\hat{\theta}\hat{\theta}}^\pm = K_{\hat{\phi}\hat{\phi}}^\pm = \frac{v_f f(R_H) + M_0 R_H}{R_H M_\pm(v)\sqrt{v_f (v_f f(R_H) + 2M_0 R_H)}}. \quad (\text{E17c})$$

Introducing the discontinuity in the extrinsic curvature as $[K_{ij}] := K_{ij}^+ - K_{ij}^-$, we have

$$[K_{\hat{t}\hat{t}}] = -\frac{M_0 R_H f'(R_H)}{M_\Gamma f(R_H)\sqrt{v_f [v_f f(R_H) + 2M_0 R_H]}}, \quad (\text{E18})$$

and $[K_{\hat{\theta}\hat{\theta}}] = [K_{\hat{\phi}\hat{\phi}}] = 0$, where M_Γ denotes the mass function on Γ , i.e., $M_-(v) = M_+(u) = M_\Gamma$. If we choose R_H that satisfies $f(R_H) > 0$ and $f'(R_H) > 0$, the value of $[K_{\hat{t}\hat{t}}]$ is negative.

On the singular hypersurface Γ , there exists distributional energy-momentum tensor (i.e. the surface stress tensor), and its specific form is determined once a theory of gravity is given. To realize the regularized spacetimes, we consider that the theory of gravity must be modified from the theory of general relativity, but an explicit calculation for the surface stress tensor in such a theory is postponed as a future issue. Instead, here we present the formula for the surface stress tensor in the framework of general relativity. This formula is expected to hold at the distant region $r \gg \ell$, because the theory of general relativity gives a good approximation in the domain where the curvature is small.

The surface stress tensor S_{ij} can be calculated using Israel's junction condition [47],

$$-8\pi G S_{ij} = [K_{ij}] - [K]\eta_{ij}. \quad (\text{E19})$$

A calculation gives $S_{\hat{t}\hat{t}} = 0$ and $S_{\hat{\theta}\hat{\theta}} = S_{\hat{\phi}\hat{\phi}} = -[K_{\hat{t}\hat{t}}]/8\pi$. Therefore, the surface Γ has no surface energy density and has negative tension. This situation is similar to Hayward's model of Ref. [9].

E.2. Non-self-similar case

We now turn our attention to the non-self-similar case. The explicit construction of the evaporation model would require numerical calculation, and here, we just discuss the basic method for this procedure. The function $F_-(v, r)$ is the same as Eq. (58) but $M(v)$ and $Q(v)$ are replaced by $M_-(v)$ and $Q_-(v)$ with $Q_-(v) = qM_-(v)$. The mass function $M_-(v)$

is given by Eq. (68), and the duration of the Hawking radiation measured in the advanced time v is denoted by v_f . We assume $F_+(u, r)$ to have the same form as $F_-(v, r)$ but $M_-(v)$ and $Q_-(v)$ being replaced by $M_+(u)$ and $Q_+(u)$, respectively:

$$F_+(u, r) = 1 - \frac{(2M_+(u)r - Q_+(u)^2)r^2}{r^4 + (2M_+(u)r + Q_+(u)^2)\ell^2}, \quad (\text{E20})$$

with $Q_-(u) = qM_-(u)$.

One must first specify the timelike hypersurface Γ on which two spacetimes are glued by choosing the function $v = v_-(r)$ in the ingoing Vaidya region. A natural choice of Γ would be a timelike hypersurface outside of the apparent horizon that satisfies $v_-(r) \rightarrow v_f$ at $r \rightarrow 0$. Once such a hypersurface Γ is specified, we require the continuity of the mass function on it, i.e. $M_-(v_-(r)) = M_+(u_+(r))$. This leads to the continuity of the functions $F_-(v, r)$ and $F_+(u, r)$ on Γ , $F_-(v_-(r), r) = F_+(u_+(r), r)$. Then, Eq. (E1) is formally solved as

$$u_+(r) = v_-(r) - 2 \int_{r_0}^r \frac{dr}{F_-(v_-(r), r)}, \quad (\text{E21})$$

where r_0 denotes the radius of Γ at $v = 0$ and the solution that satisfies $u'_+(r) < 0$ is chosen. The duration u_f of the Hawking radiation measured in the retarded time is

$$u_f := u_+(0) = v_f + 2 \int_0^{r_0} \frac{dr}{F_-(v_-(r), r)}. \quad (\text{E22})$$

Once the function $u = u_+(r)$ is obtained, one can consider its inverse function $r = r_+(u)$. Then, the mass function $M_+(u)$ is determined as

$$M_+(u) = M_-(v_-(r_+(u))). \quad (\text{E23})$$

We calculate the surface stress tensor of the hypersurface Γ . In the same way as the self-similar case, we introduce the coordinates $z_+ = u$ and $z_- = v$, and then, the metrics are given by Eq. (E10). In addition, we introduce the function $\tilde{z}_+(r) = u_+(r)$ and $\tilde{z}_-(r) = v_-(r)$. In the $(z_{\pm}, r, \theta, \phi)$ coordinates, the unit normal to Γ is calculated as

$$n_{\mu}^{\pm} = \frac{1}{\sqrt{\tilde{z}'_{\pm}(F_{\pm}\tilde{z}'_{\pm} \pm 2)}} (1, -\tilde{z}'_{\pm}, 0, 0), \quad (\text{E24})$$

and the triad basis on Γ is introduced as

$$\hat{t}^{\mu} = -\frac{1}{\sqrt{\tilde{z}'_{\pm}(F_{\pm}\tilde{z}'_{\pm} \pm 2)}} (\tilde{z}'_{\pm}, 1, 0, 0), \quad (\text{E25})$$

$$\hat{\theta}^{\mu} = \frac{1}{r} (0, 0, 1, 0), \quad (\text{E26a})$$

$$\hat{\phi}^{\mu} = \frac{1}{r \sin \theta} (0, 0, 0, 1). \quad (\text{E26b})$$

The extrinsic curvature on Γ calculated with the outgoing and ingoing Vaidya metrics, K_{ij}^+ and K_{ij}^- respectively, are

$$K_{\hat{t}\hat{t}}^{\pm} = -\frac{2\tilde{z}''_{\pm} \mp (\tilde{z}'_{\pm})^2 [3F_{\pm,r} + (F_{\pm,z_{\pm}} \pm F_{\pm}F_{\pm,r}) \tilde{z}'_{\pm}]}{2 [\tilde{z}'_{\pm}(F_{\pm}\tilde{z}'_{\pm} \pm 2)]^{3/2}}, \quad (\text{E27a})$$

$$K_{\hat{\theta}\hat{\theta}}^{\pm} = K_{\hat{\phi}\hat{\phi}}^{\pm} = -\frac{F_{\pm}\tilde{z}'_{\pm} \pm 1}{r\sqrt{\tilde{z}'_{\pm}(F_{\pm}\tilde{z}'_{\pm} \pm 2)}}. \quad (\text{E27b})$$

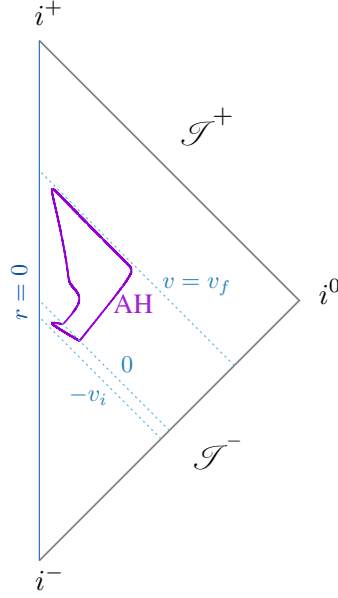


Fig. F1 Penrose diagram for the same setup as that of Fig. 13 but drawn in a different way.

Using the relation $u'_+ = v'_- - 2/F_-$, $F_- = F_+$, $F_{-,r} = F_{+,r}$, and $F_{-,v}v'_- = F_{+,u}u'_+$ that hold on Γ , the discontinuity in the extrinsic curvature is calculated as

$$[K_{\hat{t}\hat{t}}] = \frac{F_{-,v}v'_-}{F_- \sqrt{v'_-(F_-v'_- - 2)}}, \quad (\text{E28})$$

and $[K_{\hat{\theta}\hat{\theta}}] = [K_{\hat{\phi}\hat{\phi}}] = 0$. Then, similarly to the self-similar case, Israel's junction condition indicates that the surface Γ has no surface energy density and has nonzero tension in the framework of general relativity.

F. Penrose diagram drawn in a different way

In the Penrose diagram of Fig. 13, the location of the inner boundary of the trapped region and that of $r = 0$ seem to approximately coincide. This is because of the effect of the adopted advanced time u , and these two are, in fact, located at different positions. In this Appendix, we present the Penrose diagram drawn in a different way to show this point.

In this Appendix, we denote the advanced time as \tilde{u} . Each outgoing null geodesic gives the \tilde{u} -constant surface, and the value of \tilde{u} is determined by requiring $\tilde{u} = v$ at the center $r = 0$. Then, the compactified coordinates η and ζ are introduced by the same formulas as Eqs. (70a) and (70b) except that u is replaced by \tilde{u} . The worldline of the center $r = 0$ becomes a straight vertical line in this method. The Penrose diagram drawn in this way is presented in Fig. F1. In this diagram, the inner boundary of the trapped region and the center $r = 0$ are clearly separated. A similarity to Fig. 4(a) can be recognized.

References

- [1] S. W. Hawking, Nature **248**, 30-31 (1974).
- [2] S. W. Hawking, Commun. Math. Phys. **43**, 199-220 (1975) [erratum: Commun. Math. Phys. **46**, 206 (1976)].

-
- [3] S. Chakraborty and K. Lochan, *Universe* **3**, no.3, 55 (2017) [arXiv:1702.07487 [gr-qc]].
 - [4] H. Kodama, *Prog. Theor. Phys.* **63**, 1217 (1980).
 - [5] Y. Kuroda, *Prog. Theor. Phys.* **71**, 1422 (1984).
 - [6] S. W. Hawking, *Phys. Rev. D* **14**, 2460-2473 (1976).
 - [7] S. Raju, *Phys. Rept.* **943**, 1-80 (2022) [arXiv:2012.05770 [hep-th]].
 - [8] X. Calmet and S. D. H. Hsu, *EPL* **139**, no.4, 49001 (2022) [arXiv:2207.08671 [hep-th]].
 - [9] S. A. Hayward, *Phys. Rev. Lett.* **96**, 031103 (2006) [arXiv:gr-qc/0506126 [gr-qc]].
 - [10] V. P. Frolov, *JHEP* **05**, 049 (2014) [arXiv:1402.5446 [hep-th]].
 - [11] V. P. Frolov and G. A. Vilkovisky, *Phys. Lett. B* **106**, 307-313 (1981).
 - [12] T. A. Roman and P. G. Bergmann, *Phys. Rev. D* **28**, 1265-1277 (1983).
 - [13] C. Bambi, D. Malafarina and L. Modesto, *Eur. Phys. J. C* **74**, 2767 (2014) [arXiv:1306.1668 [gr-qc]].
 - [14] C. Rovelli and F. Vidotto, *Int. J. Mod. Phys. D* **23**, no.12, 1442026 (2014) [arXiv:1401.6562 [gr-qc]].
 - [15] C. Bambi, D. Malafarina and L. Modesto, *JHEP* **04**, 147 (2016) [arXiv:1603.09592 [gr-qc]].
 - [16] V. P. Frolov and A. Zelnikov, *Phys. Rev. D* **95**, no.4, 044042 (2017) doi:10.1103/PhysRevD.95.044042 [arXiv:1612.05319 [hep-th]].
 - [17] V. P. Frolov and A. Zelnikov, *Phys. Rev. D* **95**, no.12, 124028 (2017) [arXiv:1704.03043 [hep-th]].
 - [18] H. Kawai and Y. Yokokura, *Universe* **3**, no.2, 51 (2017) [arXiv:1701.03455 [hep-th]].
 - [19] P. Binétruy, A. Helou and F. Lamy, *Phys. Rev. D* **98**, no.6, 064058 (2018) [arXiv:1804.03912 [gr-qc]].
 - [20] P. M. Ho and Y. Matsuo, *JHEP* **06**, 057 (2019) [arXiv:1905.00898 [gr-qc]].
 - [21] H. Kawai and Y. Yokokura, *Universe* **6**, no.6, 77 (2020) [arXiv:2002.10331 [hep-th]].
 - [22] S. Brahma and D. h. Yeom, *Eur. Phys. J. C* **80**, no.8, 713 (2020) [arXiv:1906.06022 [gr-qc]].
 - [23] W. A. Hiscock, *Phys. Lett. A* **83**, 110-112 (1981).
 - [24] E. Poisson and W. Israel, *Phys. Rev. D* **41**, 1796-1809 (1990).
 - [25] A. Ori, *Phys. Rev. Lett.* **67**, 789-792 (1991).
 - [26] Y. Kaminaga, *Class. Quant. Grav.* **7**, 1135-1162 (1990).
 - [27] O. Levin and A. Ori, *Phys. Rev. D* **54**, 2746-2752 (1996).
 - [28] M. K. Parikh and F. Wilczek, *Phys. Lett. B* **449**, 24-29 (1999). [arXiv:gr-qc/9807031 [gr-qc]].
 - [29] S. E. Hong, D. i. Hwang, E. D. Stewart and D. h. Yeom, *Class. Quant. Grav.* **27**, 045014 (2010) [arXiv:0808.1709 [gr-qc]].
 - [30] A. Ori, *Class. Quantum Grav.* **8**, 1559 (1991).
 - [31] I. Booth, *Phys. Rev. D* **93**, 084005 (2016) [arXiv:1510.01759 [gr-qc]].
 - [32] S. Chatterjee, S. Ganguli and A. Virmani, *Gen. Rel. Grav.* **48**, no.7, 91 (2016) [arXiv:1512.02422 [gr-qc]].
 - [33] B. Creelman and I. Booth, *Phys. Rev. D* **95**, no.12, 124033 (2017) [arXiv:1610.08793 [gr-qc]].
 - [34] V. P. Frolov, *Phys. Rev. D* **94**, no.10, 104056 (2016) [arXiv:1609.01758 [gr-qc]].
 - [35] W. B. Bonnor and P. C. Vaidya, *Gen. Rel. Grav.* **1**, 127-130 (1970).
 - [36] S. A. Hayward, *Phys. Rev. D* **49**, 6467-6474 (1994).
 - [37] S. W. Hawking and G. F. R. Ellis, *The Large Scale Structure of Space-Time* (Cambridge University Press, Cambridge, UK, 1973).
 - [38] H. Maeda and T. Harada, *Class. Quant. Grav.* **39**, 195002 (2022) [arXiv:2205.12993 [gr-qc]].
 - [39] H. Maeda, *JHEP* **11**, 108 (2022) doi:10.1007/JHEP11(2022)108 [arXiv:2107.04791 [gr-qc]].
 - [40] B. Carter, *Phys. Rev. Lett.* **33**, 558-561 (1974).
 - [41] D. N. Page, *Phys. Rev. D* **16**, 2402-2411 (1977).
 - [42] W. A. Hiscock and L. D. Weems, *Phys. Rev. D* **41**, 1142 (1990).
 - [43] C. M. Chen, Y. Chen, A. Ishibashi, N. Ohta and D. Yamaguchi, *Phys. Rev. D* **105**, no.10, 106026 (2022) [arXiv:2204.09892 [hep-th]].
 - [44] J. M. M. Senovilla and R. Torres, *Class. Quant. Grav.* **32**, no.8, 085004 (2015) [erratum: *Class. Quant. Grav.* **32**, no.18, 189501 (2015)] [arXiv:1409.6044 [gr-qc]].
 - [45] R. Carballo-Rubio, F. Di Filippo, S. Liberati, C. Pacilio and M. Visser, *JHEP* **07**, 023 (2018) [arXiv:1805.02675 [gr-qc]].
 - [46] A. Bonanno and F. Saueressig, [arXiv:2211.09192 [gr-qc]].
 - [47] W. Israel, *Nuovo Cim. B* **44S10**, 1 (1966) [erratum: *Nuovo Cim. B* **48**, 463 (1967)]